Spatial Patterns and Driving Mechanisms of mid-Holocene Moisture in the Western United States: Comparison of Paleoclimate Records and Global Circulation Models

By

Nicholas Wayne Hermann

Thesis
Submitted to the Faculty of the
Graduate School of Vanderbilt University
in partial fulfillment of the requirements
for the degree of

MASTER OF SCIENCE
in

Earth and Environmental Sciences
May 2016
Nashville, Tennessee

Approved:

Jessica L. Oster, Ph.D.

Maria Luisa S.P. Jorge, Ph.D.

ACKNOWLEDGEMENTS

I would like to acknowledge and thank the Vanderbilt EES department for helping me grow both personally and as a scientist. I especially want to thank my adviser, Dr. Jessica Oster for always pushing me to do good science and being supportive when my path was bumpy. You gave me the perfect Master’s experience, and I will always be grateful for everything you have helped me learn and achieve. Dan Ibarra, thank you so much for helping me figure out how to program. I also want to thank my awesome research group members/cave buddies, Aaron Covey, and Izzy Weisman; Lydia Harmon for being a wonderful friend and roommate; Jen Bradham for being the best organizer I have ever met; Dr. Ralf Bennartz and John Rausch for teaching me how to read and understand NetCDF files; my committee members, Dr. Malu Jorge and Dr. Larissa DeSantis; and all of the EES graduate students and faculty that I have had the privilege to interact with over the past two years. I would not be where I am today without each and every one of you, and I will never forget my amazing Vandy EES family.

Additionally, I want to thank all of my family and friends who have been there for me throughout this entire journey. Eric Stevens, thank you for recommending Vanderbilt as a potential grad school; it was definitely the best choice! Joe Weller, you are the best bartender in Tennessee and a great man; thanks for your support and encouragement. To my friends back home and across the country, thank you for the moral support and love, especially Emily Chatmas, Kevin Theissen, Tom Hickson, Lisa Lamb, Katrina Korman, and Brady Ziegler. A special thanks to Josh Bear, Nate Ruppert, Joe Sinniger, Mark Weise, Shelby Dahl, and Brandi Grimm, whose visit meant the world to me! Mom, Dad, Hermanns, Smiths, and family everywhere, thank you for the love and support! Finally, I want to thank my best friend, Ana Schanzenbach, who has always been the biggest cheerleader in my life. I love you all!

TABLE OF CONTENTS

LIST OF TABLES

LIST OF FIGURES

INTRODUCTION

The western United States is a mosaic of diverse vegetation, soils, topography, and hydrology. Today, it is home to a substantial portion of the nation's agricultural land and population. California alone accounts for 12% of the U.S. population (U.S. Census Bureau 2016) and agricultural sector output of the U.S. economy (USDA ERS 2016). As a whole, eight of the western states (WA, OR, CA, NV, AZ, UT, NM, ID) contain 23% of the farmed land, 20% of the agricultural output, and 21% of the population in the country. Surface water usage constitutes 91% of total water withdrawals for the West (Maupin et al 2010) and is highly sensitive to changing precipitation and temperature. Anthropogenic warming is expected to raise global temperatures 1-2°C within the next century (IPCC 2014), potentially increasing evaporation rates and taxing crucial surface water resources. However, future changes in precipitation patterns are less certain because of high natural variability within the climate system (IPCC 2014). Given the hydrologic sensitivity, agricultural significance, and high water demand in the West, it is critical to understand the mechanisms that have driven past periods of drought, and how these are manifested spatially across the West to predict what might possibly occur in the future.

California recently suffered the worst moisture deficit seen in the past 1200 years, as indicated by historical and tree ring records (Griffin and Anchukaitis 2014). The primary driver of the severity of the recent drought (2012-2015) is thought to be significantly high temperature anomalies leading to higher evaporation rates co-occurring with low, but not unusual, precipitation levels (Griffin and Anchukaitis 2014; Diffenbaugh et al., 2015). The precipitation deficit resulted from the formation of a resilient high pressure ridge that diverted moisture north of California and much of the western U.S. coast (Swain et al 2014). It is unclear from climate models of future scenarios whether similar high pressure ridging and drought is a natural feature of the climate system (Seager et al., 2014), or one that will be and has been exacerbated with anthropogenic warming (Swain et al., 2014). Thus, the influence of future warming on drought frequency and intensity in the West is uncertain.

Terrestrial climate archives suggest widespread aridity was a persistent feature of western North American climate during the mid-Holocene (8.2-3.5kyr BP) (Thompson et al 1993), a time of greater summer insolation and lower winter insolation than present. Although the boundary conditions between the mid-Holocene and the present differ, investigating the driving mechanisms of mid-Holocene aridity may shed light on the prospects of drought in a warmer world. While general (global) and regional circulation models (GCMs and RCMs, respectively) reproduce the sign of temperature patterns during the mid-Holocene, previous model-proxy comparisons have suggested that these models have difficulty predicting the precipitation changes noted in the proxy record (Diffenbaugh and Sloan 2004, Harrison et al 2014). However, these previous model-proxy comparisons have focused on global model-proxy agreement (Harrison et al 2014), used qualitative vs. quantitative comparisons (Thompson et al 1993; Mock and Brunelle Daines 1999; Diffenbaugh and Sloan 2004), drawn climate information from a single proxy type (Harrison et al 2014), or used too few paleoclimate records to sufficiently characterize the western U.S. (Harrison et al 2014; Diffenbaugh and Sloan 2004). To reconcile these issues, I have conducted a systematic comparison of the annual and seasonal precipitation and effective moisture results from twelve mid-Holocene GCM simulations to a diverse collection of 164 mid-Holocene moisture-sensitive proxy records from the western U.S. I use the Cohen's Weighted Kappa Statistic (K_w) to quantitatively assess agreement between the model output and proxy records. I then compare model-proxy agreement with atmospheric patterns to determine what large-scale processes likely drove hydroclimatic changes in the western U.S. during the mid-Holocene. The atmospheric patterns seen in the western U.S. during the mid-Holocene will help give context to periods of drought observed today and expressed by predictive models of future climate change.

BACKGROUND

COHMAP, the Cooperative Holocene Mapping Project, was an early effort to characterize changes in global climate in response to orbital position and ice sheet growth/decay in 3 kyr timeslices from 18 kyr BP to present (Kutzbach and Ruddiman 1993). This single-model time slice approach allowed for identification of large scale atmospheric patterns for comparison with precipitation and temperature estimates from proxy records. Thompson et al. (1993) compiled a thorough network of Late Glacial and Holocene paleoclimate records from the western U.S for comparison with COHMAP's NCAR CCM atmospheric-only model. In general, the model indicated that atmospheric conditions leading to the observed mid-Holocene moisture patterns in the western U.S. included a stronger North Pacific High and an enhanced monsoon in the Southwest during the summer (Thompson et al 1993). However, the CCM model had coarse resolution grid cells (4°lat x 7.5°lon., Kutzbach and Ruddiman 1993) which could not take into account the topographic complexity of the western U.S. Thompson et al. (1993) focused mainly on summer changes, typically excluding discussion of the winter season, when the West receives a significant portion of annual precipitation. Globally, these early models were valuable for assessing large scale circulation patterns and general patterns of changing atmospheric circulation, but lacked the resolution necessary to properly assess detailed moisture changes in the West.

As computational power rose, models moved forward from atmosphere-only to coupled ocean-atmosphere-vegetation models, providing dynamic interactions to variables previously prescribed, such as vegetation distribution (Bracconot et al 2012). Additionally, these newer models were run for longer time periods (100+ years [Bracconot et al 2012] vs. 5-10 years [Kutzbach and Ruddiman 1993]), allowing analysis of inter-annual and multi-decadal variability. The longer model runs especially benefit the Pacific Ocean and western North America because ocean-atmosphere interactions such as the El Niño-Southern Oscillation on 2-7 year time scales and the Pacific Decadal Oscillation on 20-70 year timescales have significant implications for the distribution and amount of precipitation reaching the West (Wise 2010).

The Paleoclimate Modelling Intercomparison Project (PMIP) emerged from COHMAP. PMIP recognized that results from models depended on the parameterization and input given to GCMs, and sought to analyze how different models performed in response to the same forcings. PMIP has produced several phases of models with increasing complexity, the most recent of which is Phase 3, or PMIP3. For the mid-Holocene simulations, all parameters were identical to the pre-industrial control (piControl) simulation except for the orbital parameters (Taylor et al 2011). A recent study compared PMIP3 model output from the Last Glacial Maximum (21 ka) and mid-Holocene (6 ka) for agreement with speleothem records of precipitation variability from around the world, finding that agreement was strongly dependent on the variable being observed (Harrison et al 2014). However, this comparison included only three records from the U.S., and none west of the Rocky Mountains and is therefore insufficient to understand the ability of PMIP3 models to simulate proxy-inferred changes in moisture and temperature in this region during the mid-Holocene. Analysis of an RCM of the western U.S. indicates that although temperature changes in the mid-Holocene are well-represented in the model, effective moisture (precipitation – evaporation) shows poor agreement with the proxy record (Diffenbaugh and Sloan 2004). In this study, I statistically compared a large collection of mid-Holocene moisture-sensitive proxy records from the western U.S. against PMIP3 GCM simulations to assess agreement and to determine potential atmospheric drivers of climate change during the mid-Holocene.

METHODOLOGY

I compiled a network of 164 published moisture-sensitive proxy records from the western United States that cover the mid-Holocene (Figure 1, Table 1). I defined mid-Holocene sites as those that were shown to cover the interval 8.0-4.0 kyr BP (6.0 +/- 2.0 kyr BP) by absolute dating, or were previously classified as mid-Holocene by Thompson et al (1993). As some proxy records are interpreted to reflect variable moisture conditions through this interval, I focused on the period of time closest to 6 kyr BP for comparison with the PMIP3 mid-Holocene simulations. The network includes proxies from lake sediments, packrat middens, speleothems, and other terrestrial archives of climate change. Based on the authors' interpretation of each proxy site for the mid-Holocene, I classified sites as recording drier (D) conditions, wetter (W) conditions, or no change (NC) relative to modern.

Some locations, such as Vancouver Island, contained many sites within a small area, often from a single study (Figure 1). To prevent the over-representation of densely studied areas, I used ArcGIS to outline a 25km radius buffer around each site and combined proxy sites with overlapping buffer zones to create a new set of site coordinates manually selected at center of overlap (Figure 2). Buffer zones have been used in previous model-proxy comparisons to reduce over-representation of densely studied areas (DiNezio and Tierney 2013). Because the western U.S. is topographically complex, I used a 25km buffer radius (50km separation distance) such that local changes in altitude were not oversimplified within the proxy network. I determined the moisture classification for these aggregate sites by counting the number of overlapping sites that fall into each category (D/W/NC; Table 2). In most instances, I was able to use the category of the majority of the sites as the classification for the new "buffer site." In several cases, conflicts between D/W and NC were resolved by selecting either D or W. At two sites, there was an equal split of D and W, or a split between D, W, and NC. In both cases of equal splits, I chose to classify the buffer site as NC. The final proxy network (Figure 3) after combining sites contained 98 geographic coordinates for climate model data extraction with 64 classified as drier, 18 classified as no change, and 16 classified as wetter relative to preindustrial conditions (Table 3).

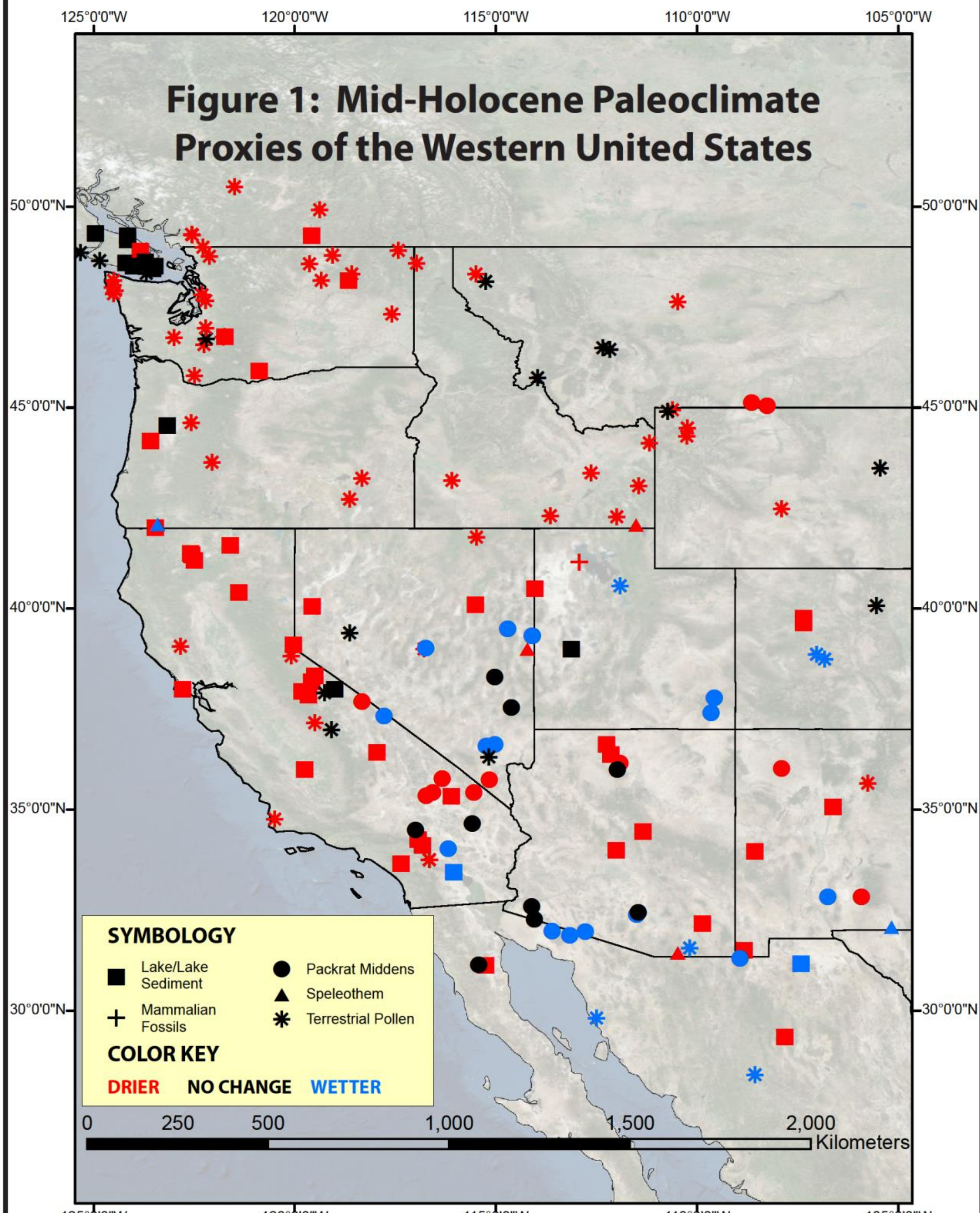

Figure 1: The observed proxy network used in this study. The majority of moisture proxies for the mid-Holocene (6 +/- 2 kyr BP) come from pollen records from lake sediments. Here, "Lake/Lake Sediments" entail studies that used proxies other than pollen or in addition to pollen, while "Terrestrial Pollen" records are lake or other terrestrial sediments that rely strictly on pollen analysis. Many of the records here are originally compiled in Thompson et al. 1993 and Metcalfe et al. 2015.

Table 1: Proxy Sites Used in κ_w Analysis				
Location	**Longitude**	**Latitude**	**Moisture Classification**	**References**
Atlatl Cave	-107.9	36.03	Drier	Betancourt and Van Devender 1981
Battle Ground Lake	-122.49	45.8	Drier	Barnosky 1985a
Blue Lake	-114.03	40.5	Drier	Louderback and Rhode 2009
Carp Lake	-120.88	45.92	Drier	Whitlock et al 2000
Cienega de Camilo	-108.57	28.42	Wetter	Ortega-Rosas et al 2008
Clear Lake	-122.84	39.07	Drier	Adam 1988
Estancia Basin	-106.62	35.07	Drier	Menking and Anderson 2003
Eureka View	-117.78	37.33	Wetter	Spaulding 1980
Glenmire	-122.78	37.99	Drier	Anderson et al 2013
Gold Lake Bog	-122.04	43.65	Drier	Sea and Whitlock 1995
Grays Lake	-111.44	43.06	Drier	Beiswenger 1991
Hidden Cave	-118.63	39.41	No Change	Wigand and Mehringer 1985
Homestead Cave	-112.93	41.16	Drier	Grayson 2000
Ice Slough	-107.9	42.48	Drier	Beiswenger 1991
Joshua Tree National Monument	-116.18	34.03	Wetter	Holmgren et al 2009
Laguna Babicora	-107.82	29.35	Drier	Roy et al 2013
Lake Cahuilla (Salton Basin)	-116.05	33.45	Wetter	Li et al 2008
Lake Cochise	-109.87	32.17	Drier	Waters 1989
Lake Elsinore	-117.35	33.66	Drier	Kirby et al 2010
Little Lake	-123.58	44.17	Drier	Worona and Whitlock 1995

Table 1: Proxy Sites Used in κ_w Analysis				
Location	**Longitude**	**Latitude**	**Moisture Classification**	**References**
Little Willow Lake	-121.39	40.41	Drier	West 2003
Mahoney Lake	-119.58	49.28	Drier	Lowe et al 1997
Marble Mountains	-115.58	34.66	No Change	Spaulding 1980
McCullough Range	-115.17	35.75	Drier	Spaulding 1991
Medicine Lake	-121.6	41.58	Drier	Starratt 2009
Mescal Mountain	-115.55	35.43	Drier	Koehler et al 2005
Mission Cross Bog	-115.48	41.78	Drier	Thompson 1984
Montezuma Well	-112	34	Drier	Davis and Shafer 1992
Owens Lake	-117.96	36.44	Drier	Bacon et al 2006
Palomas Basin	-107.42	31.17	Wetter	Castiglia and Fawcett 2006
Pink Panther Cave	-105.17	32.08	Wetter	Asmerom et al 2007
Potato Lake	-111.35	34.46	Drier	Anderson 1993
Pyramid Lake	-119.56	40.06	Drier	Benson et al 2002
Rattlesnake Cave	-112.63	43.38	Drier	Beiswenger 1991
Red Rock Lake	-105.54	40.08	No Change	Maher 1972
Ruby Lake/Marsh	-115.51	40.11	Drier	Thompson 1984
Sacramento Mountains	-105.92	32.83	Wetter	Van Devender et al 1984
San Agustin Plain	-108.57	33.97	Drier	Markgraf et al 1984
San Antonio Creek Section	-120.49	34.78	Drier	Anderson et al 2015
Sevier Lake	-113.13	39	No Change	Oviatt 1988
Sierra Bacha	-112.5	29.83	Wetter	Anderson and Van Devender 1995
Snowbird Bog	-111.92	40.58	Wetter	Madsen and

Table 1: Proxy Sites Used in κ_w Analysis				
Location	**Longitude**	**Latitude**	**Moisture Classification**	**References**
				Currey 1979
Stewart Bog	-105.75	35.67	Drier	Jimenez-Moreno et al 2008
Tulare Lake	-119.75	36	Drier	Davis et al 1999
Turtle Lake	-124.96	49.33	No Change	Brown et al 2006
Valleyview	-114.72	39.5	Wetter	Thompson 1984
White Mountains	-118.33	37.7	Drier	Jennings and Elliot-Fisk 1993
Zenkner Valley section	-123	46.75	Drier	Heusser 1977
Carlins Cave	-115.03	38.3	No Change	Thompson et al 1993
Cub Lake	-111.18	44.13	Drier	Thompson et al 1993
Diamond Pond	-118.33	43.25	Drier	Thompson et al 1993
Etna	-114.62	37.55	No Change	Thompson et al 1993
Fish Lake	-118.63	42.73	Drier	Thompson et al 1993
Goose Lake	-119.34	48.17	Drier	Thompson et al 1993
Kelowna Bog	-119.38	49.93	Drier	Thompson et al 1993
Lake Cleveland	-113.65	42.32	Drier	Thompson et al 1993
Lost Trail Pass Bog	-113.97	45.75	No Change	Thompson et al 1993
Murphey's rock shelter	-116.1	43.2	Drier	Thompson et al 1993
Pinecrest Lake	-121.5	50.5	Drier	Thompson et al 1993
Rhodes Canyon	-106.75	32.83	Wetter	Thompson et al 1993
Williams Fen	-117.58	47.33	Drier	Thompson et al 1993

Table 1: Proxy Sites Used in κ_w Analysis				
Location	**Longitude**	**Latitude**	**Moisture Classification**	**References**
1	-125.08	48.773	No Change	
2	-124.49	47.942	Drier	
3	-123.73	48.542	No Change	
4	-124.12	49.191	No Change	
5	-122.27	49.028	Drier	
6	-118.61	48.255	Drier	
7	-119.34	48.694	Drier	
8	-122.26	47.753	Drier	
9	-121.96	46.761	Drier	
10	-115.37	48.236	Drier	
11	-117.19	48.758	Drier	
12	-112.23	46.479	No Change	
13	-110.66	44.93	Drier	
14	-110.23	44.281	Drier	
15	-108.45	45.091	Drier	
16	-123.42	42.066	No Change	
17	-122.54	41.333	Drier	
18	-111.76	42.189	Drier	
19	-107.34	39.711	Drier	
20	-106.93	38.813	Wetter	
21	-109.61	37.596	Wetter	
22	-114.11	39.326	No Change	
23	-115.15	36.54	Wetter	
24	-116.77	38.999	No Change	
25	-119.47	38.074	Drier	
26	-119.29	37.086	Drier	
27	-120.04	38.963	Drier	
28	-116.5	35.473	Drier	
29	-116.85	34.151	Drier	
30	-115.34	31.151	Drier	

Table 1: Proxy Sites Used in κ_w Analysis				
Location	**Longitude**	**Latitude**	**Moisture Classification**	**References**
31	-114.08	32.439	No Change	
32	-113.18	31.98	Wetter	
33	-111.47	32.42	Wetter	
34	-112.06	36.282	Drier	
35	-108.88	31.397	No Change	
36	-110.42	31.467	No Change	
37	-122.88	44.59	Drier	

Table 1: Proxy site locations and moisture classifications for extraction of GCM data. Italicized site names are sites for which I was unable to access the original reference, and proxy interpretations come directly from the interpretation in Thompson et al 1993. Numbered sites are locations which combined multiple proxy records and are explained in detail in Table 2.

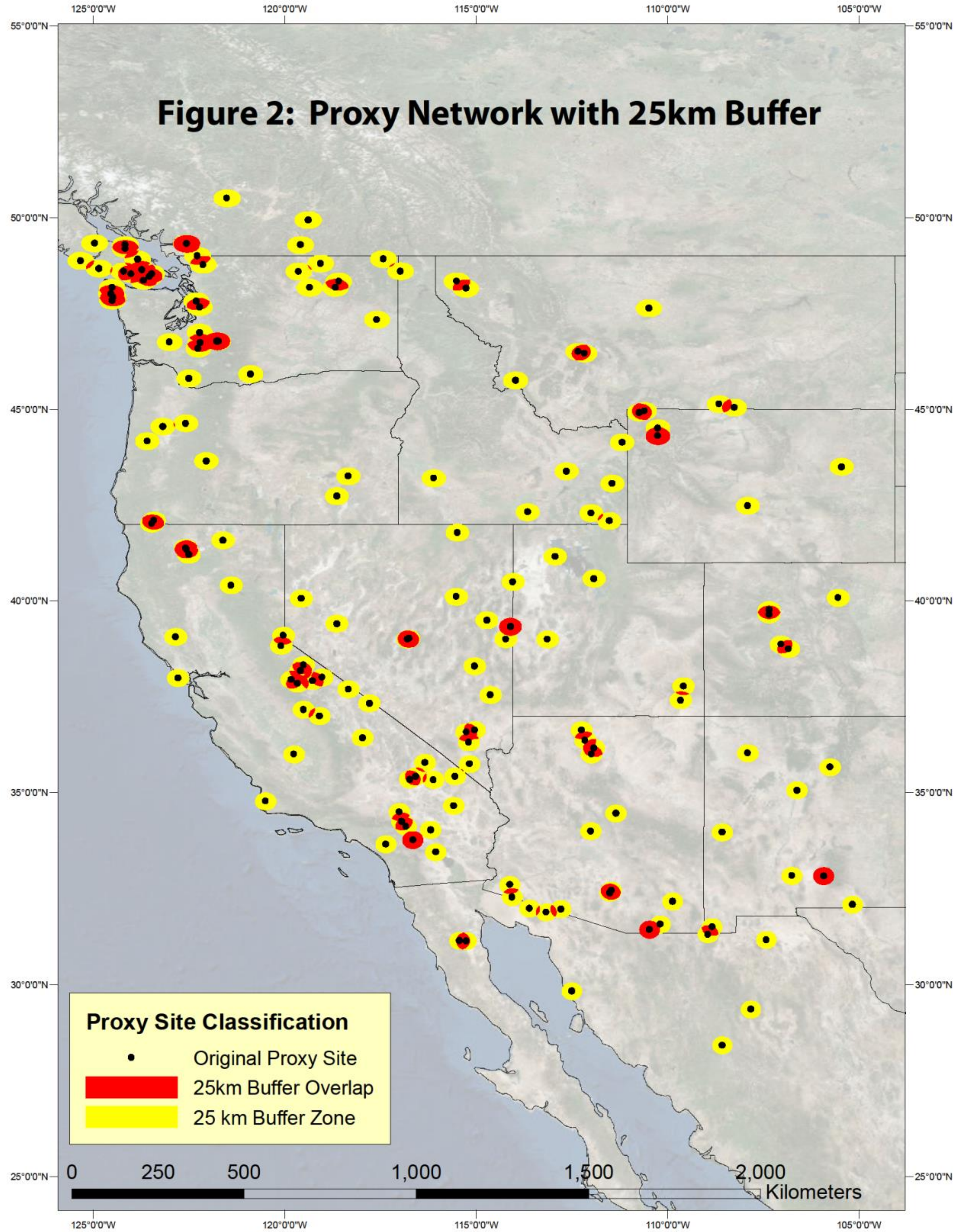

Figure 2: Original proxy network with 25km buffer zones (yellow). Areas of overlap (red) were used to identify locations where sites needed to be combined and reclassified to reduce overall proxy network density in highly studied areas.

Table 2: Aggregate Sites and Their Constituents					
Site Number (*Site Name*)	**Longitude**	**Latitude**	**Moisture Class**	**References**	**Aggregate Confidence**
1	**-125.08**	**48.773**	**No Change**		**Robust**
Effingham Island Bog	*-125.32*	*48.87*	*No Change*	*Brown et al 2006*	
Whyac Lake Bog	*-124.84*	*48.67*	*No Change*	*Brown et al 2006*	
2	**-124.49**	**47.942**	**Drier**		**Robust**
Hoh River Valley Site	*-124.50*	*47.83*	*Drier*	*Heusser 1974*	
Soleduck Bog	*-124.47*	*47.92*	*Drier*	*Heusser 1973*	
Wentworth Lake	*-124.53*	*48.01*	*Drier*	*Heusser 1973*	
Wessler Bog	*-124.50*	*48.17*	*Drier*	*Heusser 1973*	
3	**-123.73**	**48.542**	**No Change**		**Majority**
East Sooke Fen	*-123.68*	*48.35*	*No Change*	*Brown et al 2006*	
Heal Lake	*-123.47*	*48.53*	*No Change*	*Brown et al 2006*	
Langford Lake	*-123.53*	*48.45*	*No Change*	*Brown et al 2006*	
Pixie Lake	*-124.20*	*48.60*	*No Change*	*Brown et al 2006*	
Porphyry Lake	*-123.83*	*48.91*	*Drier*	*Brown and Hebda 2003*	
Rhamnus Lake	*-123.72*	*48.63*	*No Change*	*Brown et al 2006*	
Walker Lake	*-124.00*	*48.53*	*No Change*	*Brown and Hebda 2003*	
4	**-124.12**	**49.191**	**No Change**		**Robust**
Boomerang Lake	*-124.16*	*49.18*	*No Change*	*Brown et al 2006*	
Enos Lake	*-124.16*	*49.28*	*No Change*	*Brown et al 2006*	
5	**-122.27**	**49.028**	**Drier**		**Robust**
Marion Lake	*-122.55*	*49.31*	*Drier*	*Mathewes 1973*	
Mosquito Lake	*-122.12*	*48.77*	*Drier*	*Hansen and Easterbrook 1974*	
Pangborn Bog	*-122.27*	*49.00*	*Drier*	*Hansen and Easterbrook 1974*	
Surprise Lake	*-122.56*	*49.32*	*Drier*	*Mathewes 1973*	
6	**-118.61**	**48.255**	**Drier**		**Robust**
Simpson's Flatts	*-118.58*	*48.33*	*Drier*	*Thompson et al 1993*	
Waitts Lake	*-118.67*	*48.17*	*Drier*	*Thompson et al 1993*	
7	**-119.34**	**48.694**	**Drier**		**Robust**
Bonaparte Meadows	*-119.06*	*48.80*	*Drier*	*Mack et al 1979*	
Mud Lake	*-119.63*	*48.59*	*Drier*	*Mack et al 1979*	
8	**-122.26**	**47.753**	**Drier**		**Robust**
Hall Lake	*-122.30*	*47.82*	*Drier*	*Thompson et al 1993*	
Lake Washington	*-122.22*	*47.67*	*Drier*	*Leopold et al 1982*	
9	**-121.96**	**46.761**	**Drier**		**Majority**

Table 2: Aggregate Sites and Their Constituents					
Site Number (*Site Name*)	**Longitude**	**Latitude**	**Moisture Class**	**References**	**Aggregate Confidence**
Davis Lake	*-122.25*	*46.58*	*Drier*	*Barnosky 1981*	
Jay Bath	*-121.77*	*46.77*	*Drier*	*Dunwiddie 1986*	
Log Wallow	*-121.75*	*46.78*	*Drier*	*Dunwiddie 1986*	
Mineral Lake	*-122.20*	*46.73*	*No Change*	*Thompson et al 1993*	
Nisqually Lake	*-122.22*	*47.00*	*Drier*	*Thompson et al 1993*	
Reflection Pond	*-121.73*	*46.77*	*Drier*	*Dunwiddie 1986*	
10	**-115.37**	**48.236**	**Drier**		**50/50**
McKillop Creek Pond	*-115.26*	*48.15*	*No Change*	*Mack et al 1983*	
Teepee Lake	*-115.50*	*48.33*	*Drier*	*Thompson et al 1993*	
11	**-117.19**	**48.758**	**Drier**		**Robust**
Big Meadow	*-117.42*	*48.92*	*Drier*	*Mack et al 1978c*	
Hager Lake	*-116.97*	*48.60*	*Drier*	*Mack et al 1978d*	
12	-112.23	46.479	No Change		**Robust**
Forest Lake	*-112.17*	*46.45*	*No Change*	*Thompson et al 1993*	
Telegraph Creek Marsh	*-112.33*	*46.50*	*No Change*	*Thompson et al 1993*	
13	**-110.66**	**44.93**	**Drier**		**50/50**
Blacktail Pond	*-110.60*	*44.96*	*Drier*	*Beiswenger 1991*	
Gardiners Hole	*-110.73*	*44.92*	*No Change*	*Thompson et al 1993*	
14	**-110.23**	**44.281**	**Drier**		**Robust**
Buckbean Fen	*-110.25*	*44.30*	*Drier*	*Baker 1976*	
Cub Creek Pond	*-110.25*	*44.51*	*Drier*	*Waddington and Wright 1974*	
Lilypad Pond	*-110.25*	*44.30*	*Drier*	*Thompson et al 1993*	
15	**-108.45**	**45.091**	**Drier**		**Robust**
Big Pryor	*-108.65*	*45.13*	*Drier*	*Lyford et al 2002*	
East Pryor	*-108.25*	*45.05*	*Drier*	*Lyford et al 2002*	
16	**-123.42**	**42.066**	**No Change**		**Conflict Type A**
Bolan Lake	*-123.46*	*42.02*	*Drier*	*Briles et al 2005*	
Oregon Caves National Monument	*-123.41*	*42.10*	*Wetter*	*Ersek et al 2012*	
17	**-122.54**	**41.333**	**Drier**		**Robust**
Bluff Lake	*-122.56*	*41.35*	*Drier*	*Mohr et al 2000*	
Cedar Lake	*-122.50*	*41.21*	*Drier*	*Mohr et al 2000*	
Crater Lake	*-122.58*	*41.38*	*Drier*	*Mohr et al 2000*	
18	**-111.76**	**42.189**	**Drier**		**Robust**

Table 2: Aggregate Sites and Their Constituents					
Site Number (*Site Name*)	**Longitude**	**Latitude**	**Moisture Class**	**References**	**Aggregate Confidence**
Minnetonka Cave	*42.09*	*-111.52*	*Drier*	*Lundeen et al 2013*	
Swan Lake	*42.29*	*-111.99*	*Drier*	*Beiswenger 1991*	
19	**-107.34**	**39.711**	**Drier**		**Robust**
Bison Lake	*-107.35*	*39.77*	*Drier*	*Anderson 2012*	
Yellow Lake	*-107.35*	*39.65*	*Drier*	*Anderson 2012*	
20	**-106.93**	**38.813**	**Wetter**		**Robust**
Alkali Lake	*-106.83*	*38.75*	*Wetter*	*Markgraf and Scott 1981*	
Keystone Iron Bog	*-107.03*	*38.87*	*Wetter*	*Fall 1988*	
21	**-109.61**	**37.596**	**Wetter**		**Robust**
Allen Cave	*-109.58*	*37.78*	*Wetter*	*Betancourt 1984*	
Fishmouth Cave	*-109.65*	*37.42*	*Wetter*	*Betancourt 1984*	
22	**-114.11**	**39.326**	**No Change**		**Conflict Type B**
Council Hall Cave	*-114.10*	*39.33*	*No Change*	*Thompson 1984*	
Lehman Cave	*-114.22*	*39.01*	*Drier*	*Steponaitis et al 2015*	
Smith Creek Cave	*-114.10*	*39.33*	*Wetter*	*Thompson 1984*	
23	**-115.15**	**36.54**	**Wetter**		**Majority**
Desert View	*-115.03*	*36.63*	*Wetter*	*Thompson et al 1993*	
Sheep Range	*-115.25*	*36.58*	*Wetter*	*Spaulding 1980*	
Tule Springs	*-115.18*	*36.32*	*No Change*	*Thompson et al 1993*	
24	**-116.77**	**38.999**	**No Change**		**Conflict Type A**
Gatecliff Shelter	*-116.78*	*39.00*	*Drier*	*Thompson et al 1993*	
Gatecliff/June Canyon	*-116.75*	*39.02*	*Wetter*	*Thompson et al 1993*	
25	**-119.47**	**38.074**	**Drier**		**Majority**
Kirman Lake	*-119.50*	*38.33*	*Drier*	*Bloom 2006*	
Mono Lake	*-119.01*	*38.01*	*No Change*	*Davis 1999*	
Siesta Lake	*-119.66*	*37.85*	*Drier*	*Brunelle and Anderson 2003*	
Stella Lake	*-119.58*	*38.18*	*Drier*	*Reinemann et al 2009*	
Swamp Lake Yosemite	*-119.82*	*37.95*	*Drier*	*Smith and Anderson 1992*	
Tioga Pass Pond	*-119.27*	*37.92*	*No Change*	*Anderson 1990*	
26	**-119.29**	**37.086**	**Drier**		**50/50**
Balsam Meadows	*-119.50*	*37.17*	*Drier*	*Davis et al 1985*	

Table 2: Aggregate Sites and Their Constituents					
Site Number (*Site Name*)	**Longitude**	**Latitude**	**Moisture Class**	**References**	**Aggregate Confidence**
Exchequer Meadow	*-119.08*	*37.00*	*No Change*	*Thompson et al 1993*	
27	**-120.04**	**38.963**	**Drier**		**Robust**
Lake Tahoe	*-120.02*	*39.10*	*Drier*	*Lindstrom 1990*	
Osgood Swamp	*-120.08*	*38.83*	*Drier*	*Thompson et al 1993*	
28	**-116.5**	**35.473**	**Drier**		**Robust**
Ibex	*-116.33*	*35.78*	*Drier*	*Koehler et al 2005*	
Nelson Basin	*-116.73*	*35.35*	*Drier*	*Koehler et al 2005*	
No Name East	*-116.57*	*35.43*	*Drier*	*Koehler et al 2005*	
Silver Lake	*-116.11*	*35.34*	*Drier*	*Kirby et al 2015*	
29	**-116.85**	**34.151**	**Drier**		**Majority**
Big Bear Lake	*-116.94*	*34.26*	*Drier*	*Kirby et al 2012*	
Dry Lake	*-116.83*	*34.12*	*Drier*	*Bird and Kirby 2006*	
Lucerne Valley	*-117.00*	*34.50*	*No Change*	*King 1976*	
Skunk Cabbage Meadow	*-116.65*	*33.77*	*No Change*	*Wahl 2002*	
Taquitz Meadow	*-116.65*	*33.77*	*Drier*	*Wahl 2002*	
30	**-115.34**	**31.151**	**Drier**		**50/50**
Laguna Seca San Felipe	*-115.25*	*31.13*	*Drier*	*Roy et al 2010*	
Sierra San Pedro Martir	*-115.43*	*31.14*	*No Change*	*Holmgren et al 2011*	
31	**-114.08**	**32.439**	**No Change**		**Robust**
Tinajas Altas Mountains	*-114.05*	*32.28*	*No Change*	*Hall et al 1988*	
Wellton Hills	*-114.12*	*32.60*	*No Change*	*Thompson et al 1993*	
32	**-113.18**	**31.98**	**Wetter**		**Robust**
Eagle Eye Mts	*-113.17*	*31.88*	*Wetter*	*McAuliffe and Van Devender 1998*	
Hornaday Mts	*-113.60*	*31.98*	*Wetter*	*Hall et al 1988*	
Puerto Blanco Mountains	*-112.78*	*31.97*	*Wetter*	*Van Devender 1987*	
33	**-111.47**	**32.42**	**Wetter**		**50/50**
Waterman Mts	*-111.50*	*32.40*	*Wetter*	*Anderson and Van Devender 1991*	
Wolcott Peak	*-111.47*	*32.45*	*No Change*	*Thompson et al 1993*	
34	**-112.06**	**36.282**	**Drier**		**Majority**
Bear Lake	*-112.15*	*36.37*	*Drier*	*Weng and Jackson 1999*	

Table 2: Aggregate Sites and Their Constituents					
Site Number (*Site Name*)	**Longitude**	**Latitude**	**Moisture Class**	**References**	**Aggregate Confidence**
Chuar Valley	*-111.92*	*36.17*	*Drier*	*Cole 1981*	
Fracas Lake	*-112.24*	*36.63*	*Drier*	*Weng and Jackson 1999*	
Grandview Point	*-111.98*	*36.00*	*No Change*	*Cole 1981*	
35	**-108.88**	**31.397**	**No Change**		**Conflict Type A**
Lake Cloverdale	*-108.83*	*31.50*	*Drier*	*Krider 1998*	
Peloncillo Mts	*-108.94*	*31.31*	*Wetter*	*Holmgren et al 2006*	
36	**-110.42**	**31.467**	**No Change**		**Conflict Type A**
Cave of the Bells	*-110.47*	*31.43*	*Drier*	*Wagner 2006*	
Murray Springs	*-110.18*	*31.57*	*Wetter*	*Mehringer et al 1967*	
37	**-122.88**	**44.59**	**Drier**		**50/50**
Beaver Lake	*-123.18*	*44.55*	*No Change*	*Walsh et al 2010*	
Indian Prairie Fen	*-122.58*	*44.63*	*Drier*	*Sea and Whitlock 1995*	

Table 2: Sites combined using a 25km buffer radius. **Bold** sites are the aggregate locations, and *italicized* sites are the constituents. Overall, the 37 sites listed here are comprised of 103 individual proxy sites. See Table 3 for description and treatment of conflicts.

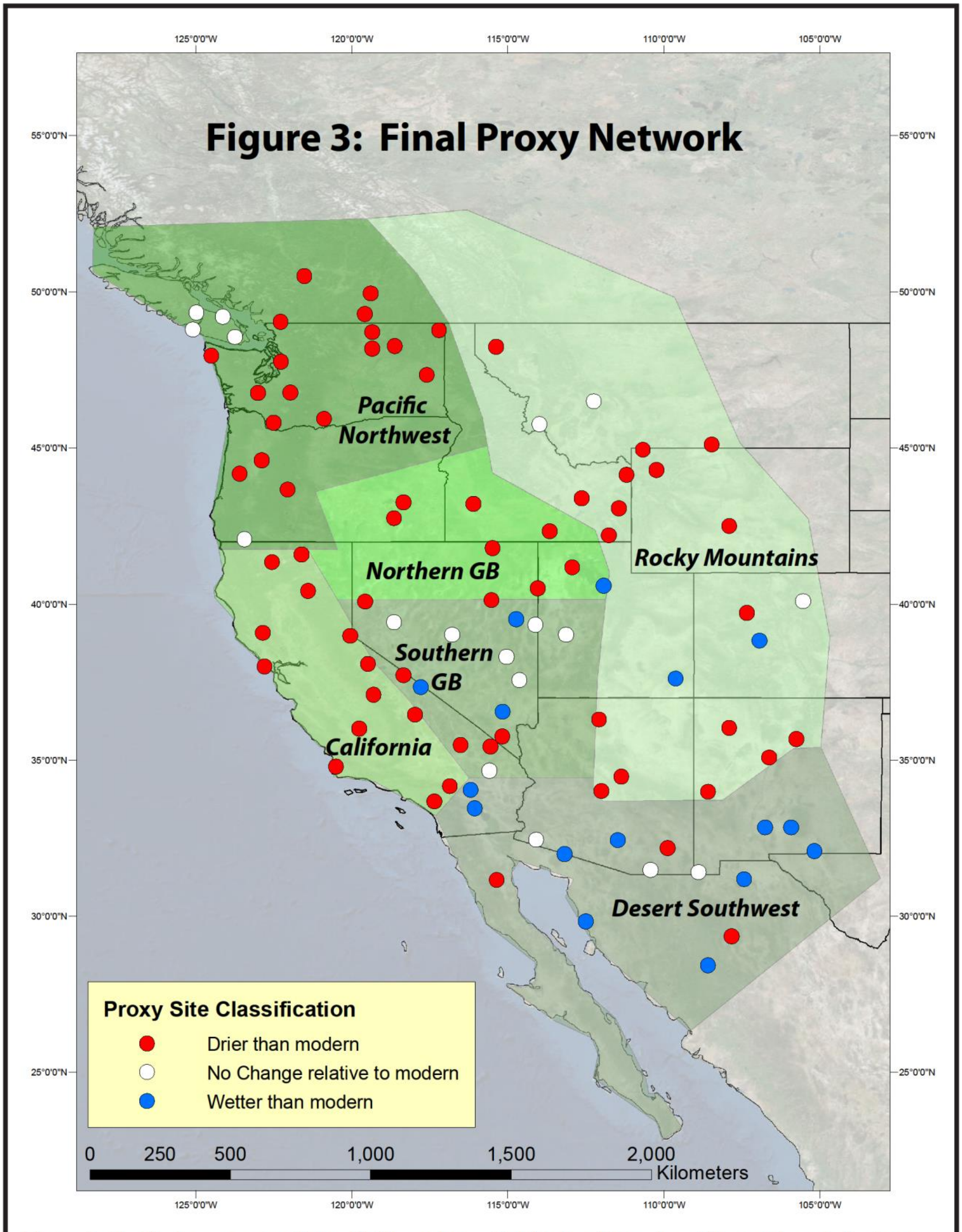

Figure 3: The final proxy network used in Kw analyses. Combining sites reduced the number of sites from 164 to 98.

Table 3: Criteria for Moisture Classification of Aggregate Sites			
Scenario	**Moisture Classification**	**Number of Occurrences**	**Justification**
All sites agree	Category of all sites	21	Majority rules
Majority of sites agree	Category of majority of sites	6	Majority rules
50/50 split between Drier/Wetter and No Change	Drier/wetter	6	Conservative estimate for disagreement
50/50 split between Drier and Wetter	No Change	4	Average of conflict indicates no change
Equal split between Drier, Wetter, and No Change	No Change	1	Average of conflict indicates no change

Table 3: The scheme used to determine the moisture classification of aggregate sites. Most aggregate sites' moisture classifications reflect either perfect or a majority agreement between constituent sites.

Using NCAR Command Language (NCL), I interpolated precipitation (P) and effective moisture (EM) values at the coordinates of each of the buffer sites from the output of the mid-Holocene (6 ka) and Pre-Industrial (0 ka) runs from twelve PMIP3 models (Table 4). Next, I calculated P and EM anomalies between the 6ka and 0ka simulations using the following equations:

$$EM_t = P_t - E_t \quad (1)$$

$$P_{Anom} = P_{6ka} / P_{0ka} * 100 \quad (2)$$

$$EM_{Anom} = EM_{6ka} / EM_{0ka} * 100 \quad (3)$$

where EM is effective moisture, P is precipitation, E is evapotranspiration, and the subscript "t" is the timeframe of interest (either 6ka or 0ka). To compare the results of the model to the proxy network, I computed the Cohen's Weighted Kappa (K_w) statistic, which measures categorical data agreement between two raters who classify items (sites) into categories (D/W/NC) relative to the probability of random agreement (Cohen 1968). Recent model-proxy intercomparisons have used the K_w statistic to analyze the ability of models to reflect precipitation changes during the Last Glacial Maximum over the Indo-Pacific (DiNezio and Tierney 2013) and the western U.S. (Oster et al 2015).

K_w is calculated using the following equation:

$$\kappa_w = 1 - \frac{\sum_{i=1}^{C} \sum_{j=1}^{C} w_{ij} x_{ij}}{\sum_{i=1}^{C} \sum_{j=1}^{C} w_{ij} m_{ij}} \quad (4)$$

where w_{ij} is the weight matrix, x_{ij} is the observed matrix, and m_{ij} is the matrix of scores expected by random chance (Cohen 1968). Here, I assigned a weight of 1 for complete disagreement (e.g. proxy says D and model says W), 0.5 for sites with moderate disagreement (e.g. proxy says NC and model says D or W), and 0 for complete agreement (e.g. proxy and model both say D). To test the robustness of agreement between models and proxies, I varied the threshold of change required for the model responses to fall into the wetter or drier category from 2-50% and calculated 95% confidence limits for the maximum K_w for each model. For example, at a threshold of 10%, a model must simulate mid-Holocene precipitation of ≥ 110 % modern for a site to be classified as wetter and ≤ 90% for a site to be classified as drier. Values from 91 – 109% modern were classified as "no change." Computed K_w values range from -1 to 1, where -1 is perfect disagreement, 0 is no agreement greater than random chance, and 1 is perfect agreement (Cohen 1968). I compared the proxy network to modeled P and EM anomaly values to generate K_w statistics for both P and EM.

Table 4: Model Spatiotemporal Resolution

Model Name	Model ID	Number of Grid Cells (Latitude)	Number of Grid Cells (Longitude)	Mid-Holocene simulation length (years)	piControl simulation length (years)
BCC-CSM1-1	BCC	64	128	100	500
CCSM4	CCSM4	192	288	301	156
CNRM-CM5	CNRM	128	256	200	850
CSIRO-MK3-6-0	CSIRO 360	96	192	100	500
CSIRO MK3L-1-2	CSIRO 312	56	64	500	1000
FGOALS-G2	FGOALS G2	60	128	686	900
FGOALS-S2	FGOALS S2	108	128	100	501
GISS-E2-R	GISS	90	144	100	1200
IPSL-CM5A-LR	IPSL	96	96	500	1000
MIROC-ESM	MIROC	64	128	100	630
MPI-ESM-P	MPI	96	192	100	1156
MRI-CGCM3	MRI	160	320	101	500

Table 4: PMIP3 models used in this study. The model ID is the shorthand code used for each model in this study. For reference, the highest resolution model (MRI) has a grid cell size of 1.25°lat x1.25°lon, and the coarsest model (CSIRO 312) has a grid cell size of 3.2°lat x 5.6°lon.

To analyze pressure system strength and position within each model run, I identified model grid cells with maximum and minimum pressures over the Pacific Ocean to locate the North Pacific High and Aleutian Low, respectively. I compared the changes in latitude, longitude, sea level pressure, and the pressure difference between the high and low with the K_w statistics for each model by 1) utilizing an Akaike information criterion for selecting the combination of variables to regress (Bartoń 2014), and then 2) performing a multiple linear regression analysis to determine whether the pressure configuration correlated with model agreement for P and EM on an annual basis. I also analyzed wind anomalies at the 250mbar and 850mbar heights to identify when and where changes in moisture advection may be occurring.

Additionally, I used the Kw statistic to compare the mid-Holocene proxy network with precipitation patterns seen in the modern California drought to determine if modern drought spatial patterns are similar to those seen in the mid-Holocene. Precipitation anomalies for the modern drought were calculated using the PRISM (Parameter elevation Regression on Independent Slopes Model) total annual precipitation dataset for 2013, the most intense year of the drought, using the following equation:

$$P_{Anom} = P_{2013} / P_{Average} *100 \quad (5)$$

where P_{2013} is the annual precipitation total for 2013 and $P_{Average}$ is the PRISM 30-year average annual precipitation amount from 1981-2010 (PRISM 2016).

RESULTS

THE MID-HOLOCENE MOISTURE PROXY RECORD

The compiled mid-Holocene proxy network indicates drier conditions over most of the study area (Figure 3). In particular, the Pacific Northwest and Northern Rockies are exclusively drier or unchanged at 6ka relative to modern. California is mostly drier at 6ka, while sites in the Great Basin and southern Rockies indicate a mixture of wetter, drier, and unchanged conditions relative to present. Proxies suggest the southwestern U.S., especially at the U.S.-Mexico border is wetter at 6ka, although much of Arizona and New Mexico are drier than modern.

MODEL ANNUAL PATTERNS

Most models show annual surface air temperatures within +/- 1°C of modern over the West and the Pacific Ocean (15-70°N, 150°E-90°W; Figure 4). However, FGOALS G2 stands out because it has annual temperatures between 0-2°C colder than modern conditions over the entire domain, including a large band of 2°C or colder anomalies over most of the area above 50°N. All models show an increase in annual P at 6ka in the Southwest (Figure 5). For other regions, the P pattern is less consistent among models. For example, half of the models show decreased or unchanged P at 6ka in the Pacific Northwest (FGOALS G2, FGOALS S2, IPSL, MIROC, MRI, and MPI), while the other half show an increase in P for the same region (BCC, CCSM4, CNRM, CSIRO_360, CSIRO_312, and GISS). Evaporation is higher in the mid-Holocene in the Southwest and northwestern Mexico in all models to some degree (Figure 6). In addition, several of the models (e.g. CSIRO_312, IPSL, MIROC, MPI) have a core region of increased evaporation values (110-120% modern) that occurs over Arizona, New Mexico, and northwestern Mexico. FGOALS G2 and FGOALS S2 both show decreased evaporation at 6ka over most of the study area, which is notably different than all other models.

Figure 4: Mean Annual Temperature Anomalies

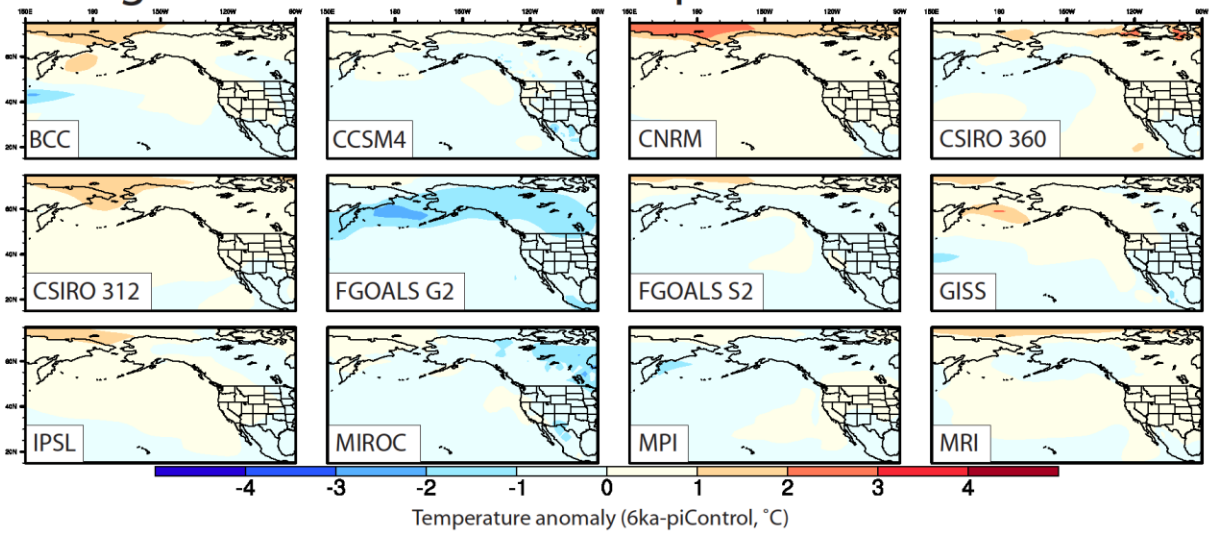

Figure 4: Mean annual temperature anomalies during the mid-Holocene for PMIP3 models.

Figure 5: Mean Annual Precipitation Anomalies

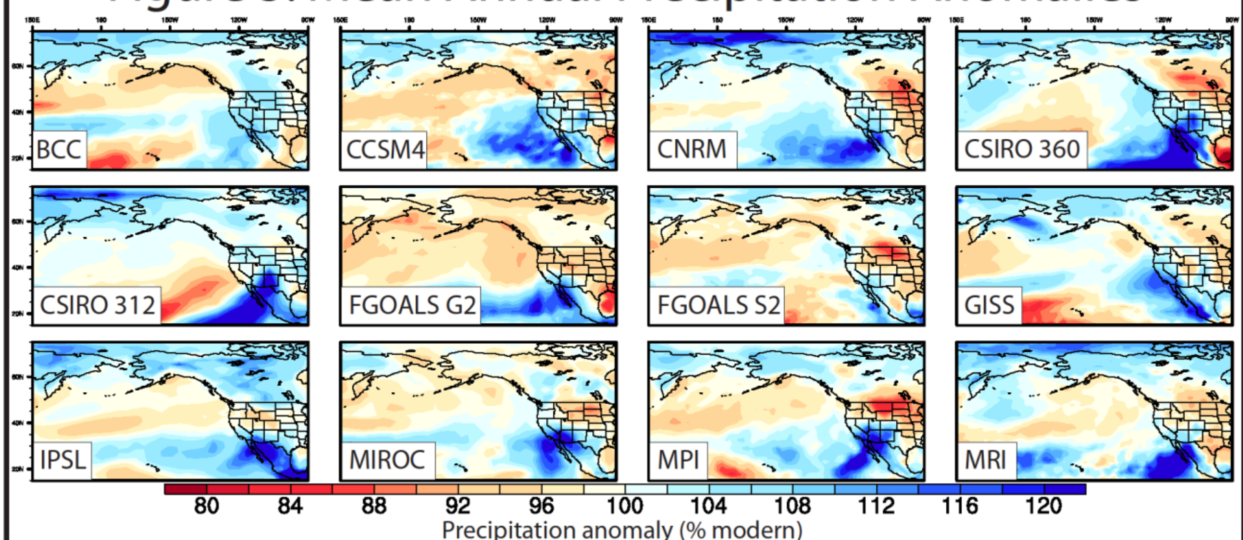

Figure 5: Mean annual precipitation anomalies during the mid-Holocene for PMIP3 models.

Modelled EM differs substantially among models (Figure 7). For example, most models indicate higher EM in the Southwest, but CCSM4 and MRI have patches of lower or unchanged EM. Three models (FGOALS G2, IPSL, and MPI) are relatively consistent with one another, having higher than modern EM in the Southwest and lower than modern EM nearly everywhere else. In particular, FGOALS G2, IPSL, and MPI have exclusively lower or near-modern EM above 42°N, whereas all other models have at least some coverage of higher EM in the Pacific Northwest and/or northern Rockies.

Figure 6: Mean Annual Evaporation Anomalies

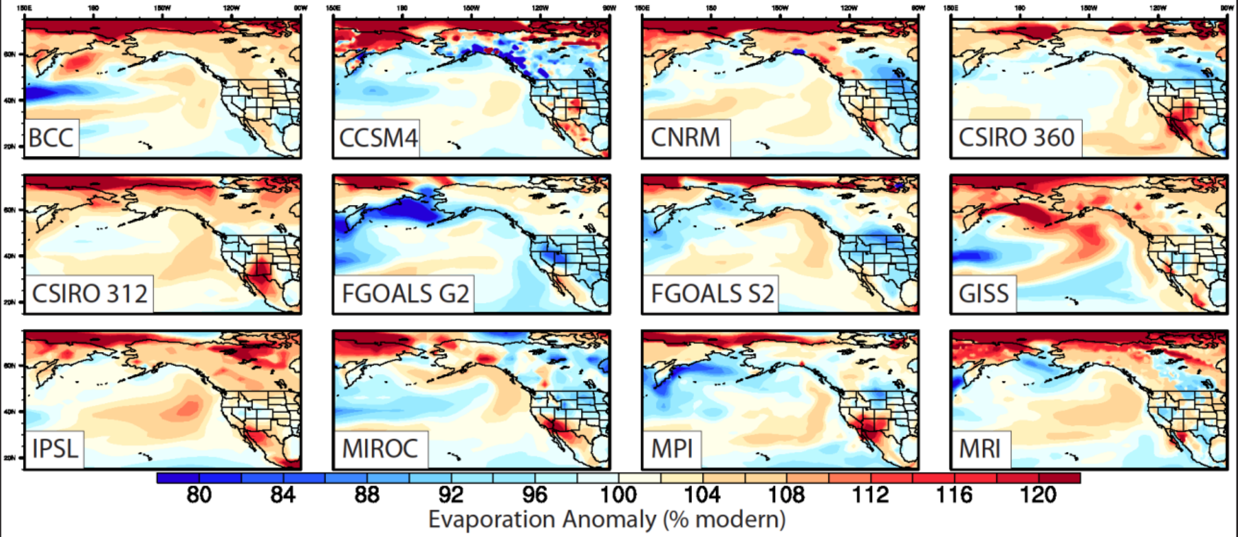

Figure 6: Mean annual evaporation anomalies during the mid-Holocene for PMIP3 models.

Figure 7: Mean Annual Effective Moisture Anomalies

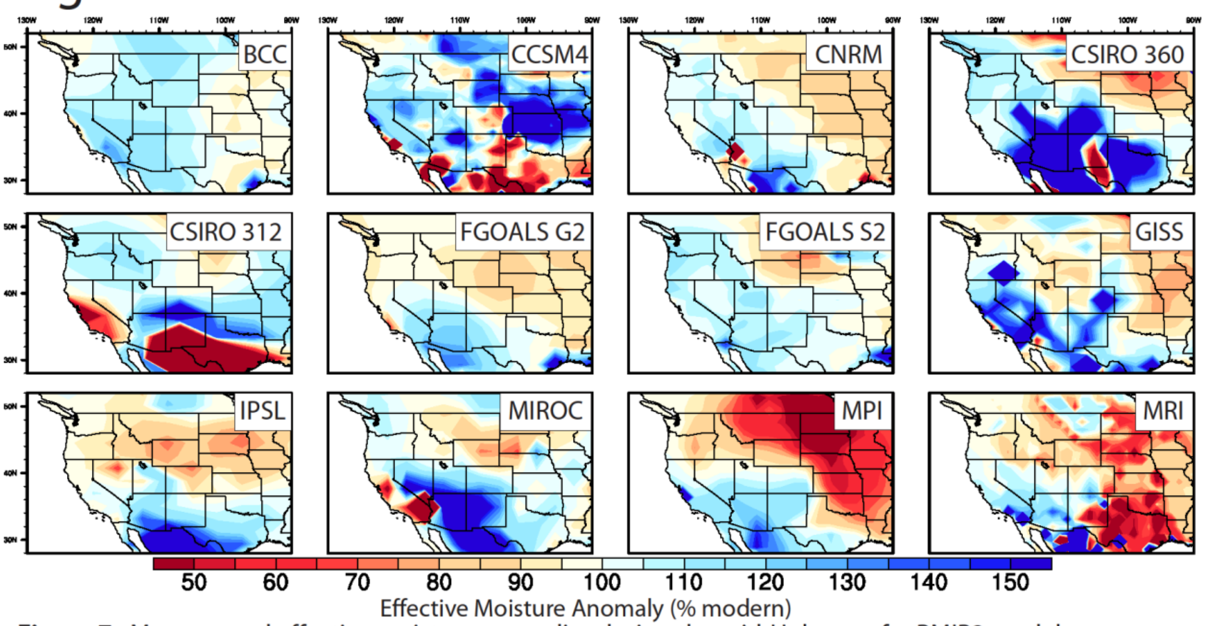

Figure 7: Mean annual effective moisture anomalies during the mid-Holocene for PMIP3 models.

Both FGOALS G2 and MPI have relatively high K_w values for P compared to other models (0.270 at the 2% threshold and 0.234 at the 2% threshold, respectively) and tend to agree with the proxy record for P in most of the Pacific Northwest and the northern Rockies, as well as near the U.S.-Mexico border (Figure 8a). FGOALS G2 and MPI show mixed agreement with the proxy network in the northern Great Basin and Rocky Mountains and generally poor agreement in most of California and along the Colorado Plateau (Figure 8a). In general, FGOALS G2 shows better agreement with the proxy network than MPI does between 37°N and 42°N, a region where most proxies indicate drier conditions, suggesting that FGOALS G2 best simulates the boundary between the dry north and wet Southwest. The remaining ten models show little to no agreement with the proxy network in Washington, California, and the Colorado Plateau (Figure 8b). However, these same ten models show better agreement with locations in the southern Great Basin which mainly are classified as NC (Figure 8b).

Figure 8: Model-Proxy Agreement by Proxy Site Based on Annual Precipitation (P)

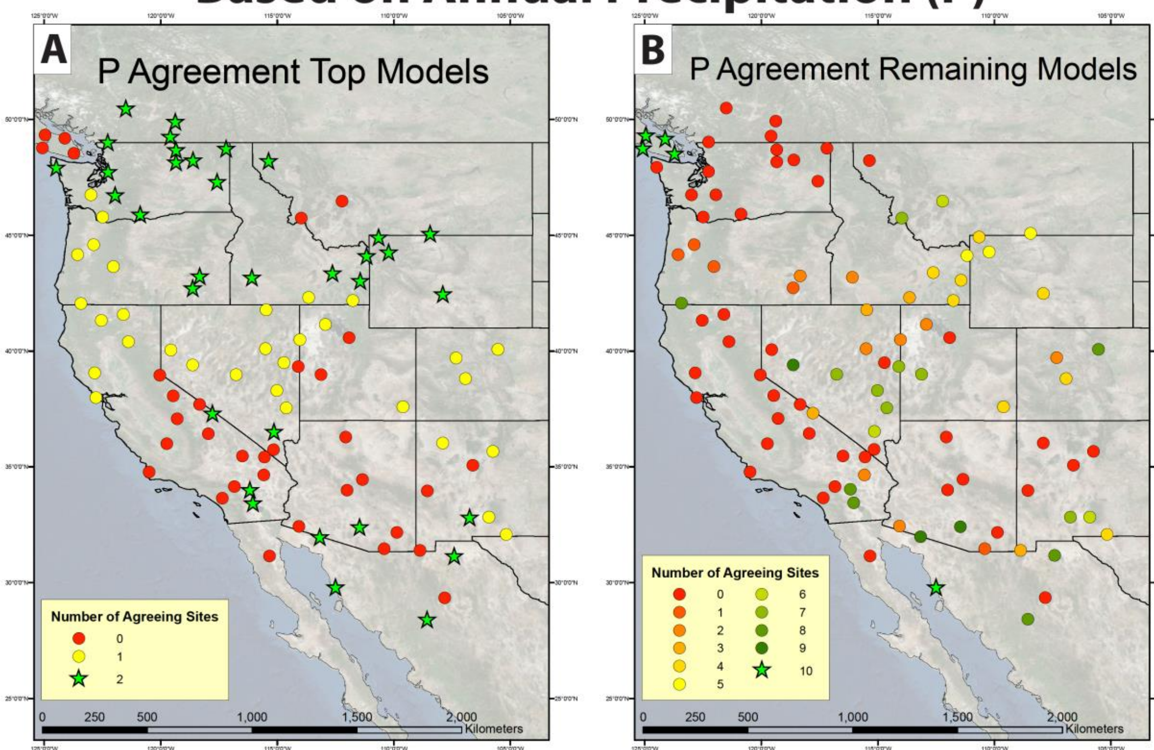

Figure 8: Number of models that show agreement for P at each proxy site for the top two (A), and the bottom ten (B) models. A) The top models based on P K_w results, FGOALS G2 and MPI, show perfect agreement with the proxy record in Washington, the northern Rockies, and the U.S.-Mexico border. B) The models with lower P K_w values perform poorly in most locations except the central Great Basin and the U.S.-Mexico border.

Overall, K_w values for EM agreement tend to be higher than K_w values for P agreement (Table 5). The models FGOALS G2, IPSL, and MPI have the highest K_w for EM (0.303, 0.279, and 0.361, respectively, all at the 2% threshold). Each of these models shows lower than modern EM in the northern U.S. and Pacific Northwest (typically above 40°N) and higher than modern EM in the Southwest (Figure 9a). Importantly, these models show excellent agreement with most sites in the Pacific Northwest and northern Rockies. The most noticeable difference between these three models is that MPI displays higher EM in California, especially along the coast, than IPSL and FGOALS G2. Some models (BCC, CCSM4, CSIRO_312, and GISS) show very poor agreement with the proxy network (K_w for EM = 0.113, -0.016, 0.016, and 0.1208, respectively) resulting from overall higher EM over most of the study area during the mid-Holocene. Although, FGOALS G2, IPSL, and MPI all have exclusively lower EM north of 42°N, all other models contain at least some areas of higher EM in this region. Similar to P, there is a clustering of non-agreement in most of California and the Colorado Plateau, a pattern that is consistent among all models (Figure 9). There is also strong agreement among all models at the U.S.-Mexico border and most of northern Mexico where models and proxies indicate wetter conditions. Once again, most of the lower nine models agree relatively well with the proxy network in the southern Great Basin where proxy records indicate EM that is similar to modern (Figure 9b).

Table 5: K_w Results and Proxy Site Agreement

Model	Max K_w	Threshold (%)	Agree	Weak Disagree	Strong Disagree
PRECIPITATION					
FGOALS G2	0.2698	2	57	23	18
MPI	0.2338	2	42	34	22
IPSL	0.1649	2	39	39	20
CSIRO 312	0.1441	10	26	64	8
MIROC	0.1437	5	29	48	21
CSIRO 360	0.1429	10	25	63	10
MRI	0.1231	2	34	44	20
FGOALS S2	0.1138	4	28	64	6
CNRM	0.1127	2	23	53	22
BCC	0.0770	6	21	64	13
GISS	0.0629	2	28	36	34
CCSM4	0.0166	10	19	78	1
EFFECTIVE MOISTURE					
Model	**Max K_w**	**Threshold (%)**	**Agree**	**Weak Disagree**	**Strong Disagree**
MPI	0.3612	2	56	23	19
FGOALS G2	0.3032	2	53	25	20
IPSL	0.2787	2	57	22	19
GISS	0.1208	40	25	67	6
CSIRO 360	0.1131	30	26	60	12
BCC	0.1113	8	24	46	28
MRI	0.1027	2	41	32	25
CNRM	0.1003	10	23	68	7
MIROC	0.0973	6	27	50	21
FGOALS S2	0.0747	8	22	62	14
CSIRO 312	0.0163	20	21	66	11
CCSM4	-0.0157	50	18	78	2

Table 5: Maximum precipitation and effective moisture Kw values and their associated thresholds for each model. Cells highlighted in green represent models that perform notably better than other models, typically showing 50% or more agreement with the proxy network. Model names highlighted in either green or purple have K_w values which are statistically significant and greater than zero at the 95% confidence interval. Non-highlighted models were not significantly different than zero.

Figure 9: Model-Proxy Agreement by Proxy Site Based on Annual Effective Moisture (EM)

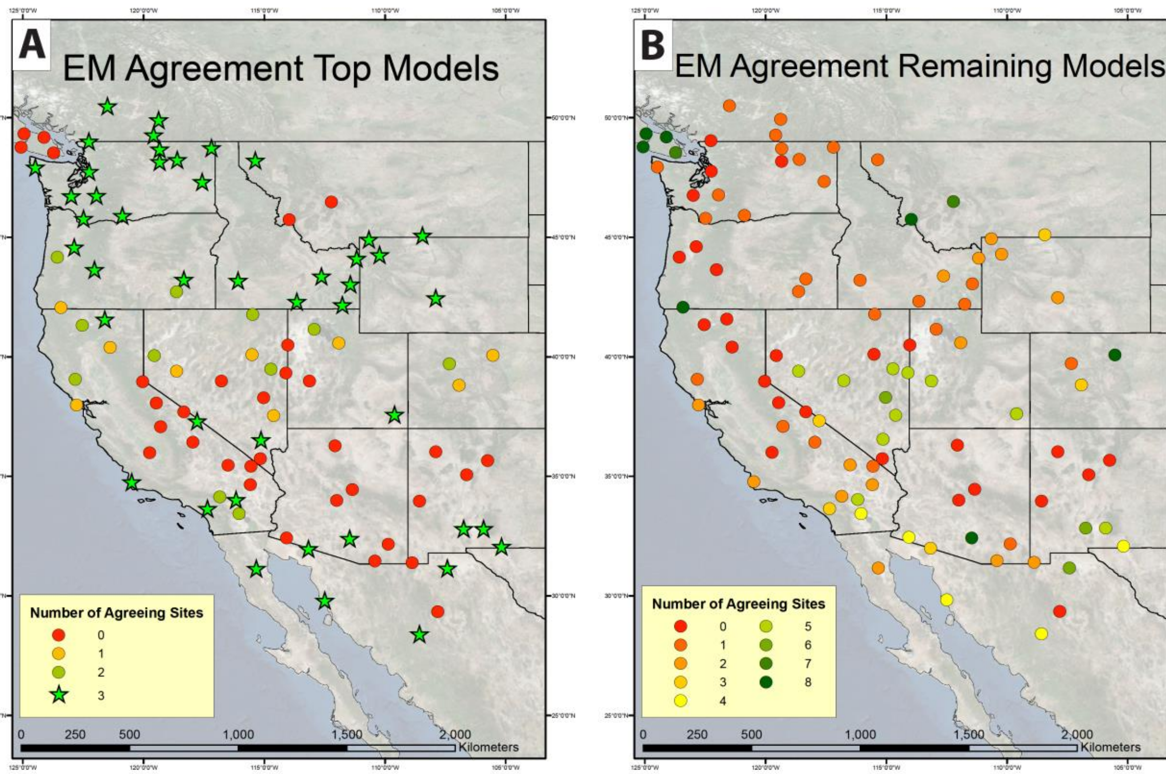

Figure 9: Number of models that show agreement for EM at each proxy site for the top three (A), and the bottom nine (B) models. A) The top three models with the highest K_w results, FGOALS G2, IPSL, and MPI, show mostly perfect agreement with the proxy record in the Pacific Northwest, northern Rockies, and the U.S.-Mexico border. The models with the lower K_w values perform poorly in most locations except the central Great Basin and the U.S.-Mexico border. B) The remaining nine models perform poorly in most locations except for the southern Great Basin and U.S.-Mexico border.

MID-HOLOCENE SEASONAL PATTERNS

Winter temperature is reduced relative to modern in all models over most or all of the study area. FGOALS G2 has the largest winter temperature decrease (1-2°C cooler than modern; Figure 10a) over most of North America, whereas all other models except MRI typically have winter temperatures between 0-1°C cooler than modern. Winter precipitation patterns indicate drier than modern conditions over almost the entire study area for FGOALS G2, the highest scoring model for P K_w (Figure 10d). IPSL and MPI show wetter winter conditions in the Pacific Northwest (Figure 10e,f). Winter evaporation is consistently lower than modern over the majority of North America across all models. FGOALS G2 is the only model to show lower than modern winter EM conditions over parts of the Pacific Northwest (Figure 10j). All other models show higher mid-Holocene EM in at least the Pacific Northwest. Models with high K_w values for annual EM (FGOALS G2, IPSL, MPI) all exhibit lower mid-Holocene EM than modern in California (Figure 10j-l), though CSIRO 360, CSIRO 360, and CNRM also have lower EM in California relative to modern.

Spring temperatures are consistently colder than modern, and FGOALS G2 once again has temperatures colder than all other models over much of North. In all models, large positive springtime P anomalies (>120% modern) persist between 20-40°N over the Desert Southwest. FGOALS G2, MPI, and IPSL all show a drier springtime Pacific Northwest (Figure 11d-f), and the former two models also have a drier northern Rocky Mountain region, similar to the spatial patterns seen in the annual P results. However, this pattern is also present in some models which show much lower agreement with the proxy network (FGOALS S2, GISS, BCC). Evaporation is similar across all models, with less evaporation in the northern study area, and increased evaporation around the Gulf of California and northwestern Mexico. Models with high annual K_w values for EM (FGOALS G2, IPSL, and MPI) all suggest at least part of the Pacific Northwest was drier than modern during the mid-Holocene spring (Figure 11j-l), though other models also show partially dry conditions there (BCC, GISS, CNRM).

All models show an increase in summer temperatures. FGOALS G2 shows lower or near-modern summer evaporation over most of the study area (Figure 12g), while all other models (except FGOALS S2) show increased summer evaporation over most or the entire region. The largest increases in summer evaporation occur over the Southwest and northern Mexico. IPSL and MPI show large (>120% modern) increases in P in the Southwest (Figure 12e,f). In contrast, FGOALS G2 shows lower summer P conditions relative to modern in almost the entire study area, with increased precipitation only occurring offshore of the west coast of Mexico (Figure 12d). Summer P does not show a consistent spatial pattern in models other than FGOALS G2, IPSL, and MPI. Additionally, all models except FGOALS G2 and GISS show positive summer EM anomalies over the entire study area relative to modern.

Autumn temperature, precipitation, and EM anomalies are generally inconsistent among all models. Among FGOALS G2, IPSL, and MPI, temperatures over most of the study area are warmer than modern (Figure 13a-c). FGOALS G2, IPSL, and MPI show lower than modern P in the northern Rockies and higher than modern P in northwestern Mexico and the Desert Southwest (Figure 13d-f). FGOALS G2 and MPI, the top performing models for K_w P, also have lower than modern P in the Pacific Northwest during the autumn months. All models except MPI and FGOALS G2 indicate higher EM than modern in the Pacific Northwest during the autumn months (Figure 13j-l). MPI and FGOALS G2 also look similar in that they have largely drier than modern conditions over most of the study area except for much of California and parts of the Southwest. In contrast to other variables, autumn evaporation is relatively consistent in most models. All models have lower-than or near-modern evaporation in the Pacific Northwest and northern Rockies, and all models except GISS and BCC have some extent of positive evaporation anomalies (110-120% modern) in the Southwest.

Figure 10: Winter (DJF) Variables for Top Performing Models

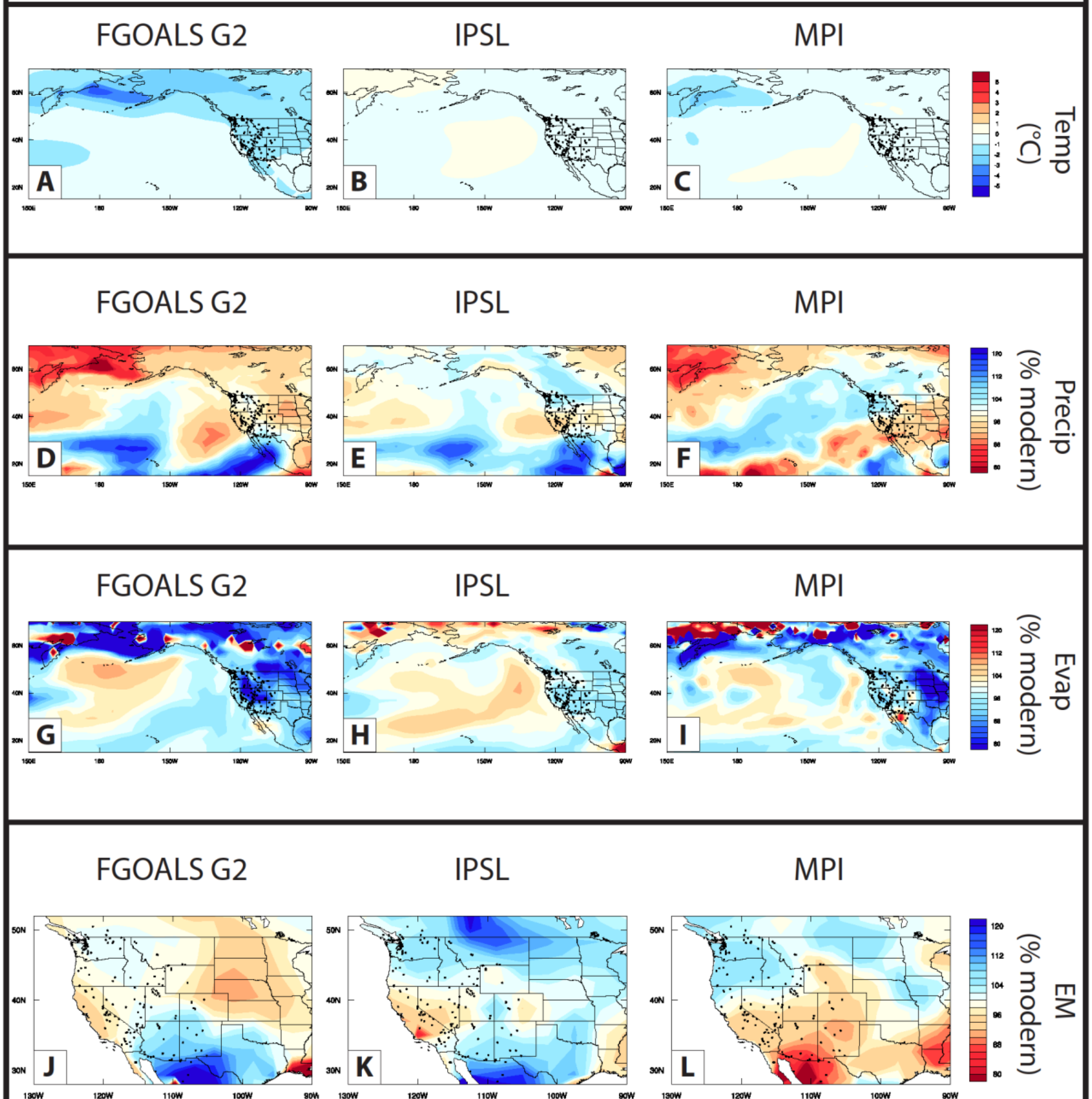

Figure 10: Mid-Holocene winter temperature anomalies (DEGREES C, A-C), precipitation anomalies (% modern, D-F), evaporation anomalies (% modern, G-I), and effective moisture anomalies (% modern, J-L) for FGOALS G2 (A,D,G,J), IPSL (B,E,H,K), and MPI (C,F,I,L).

Figure 11: Spring (MAM) Variables for Top Performing Models

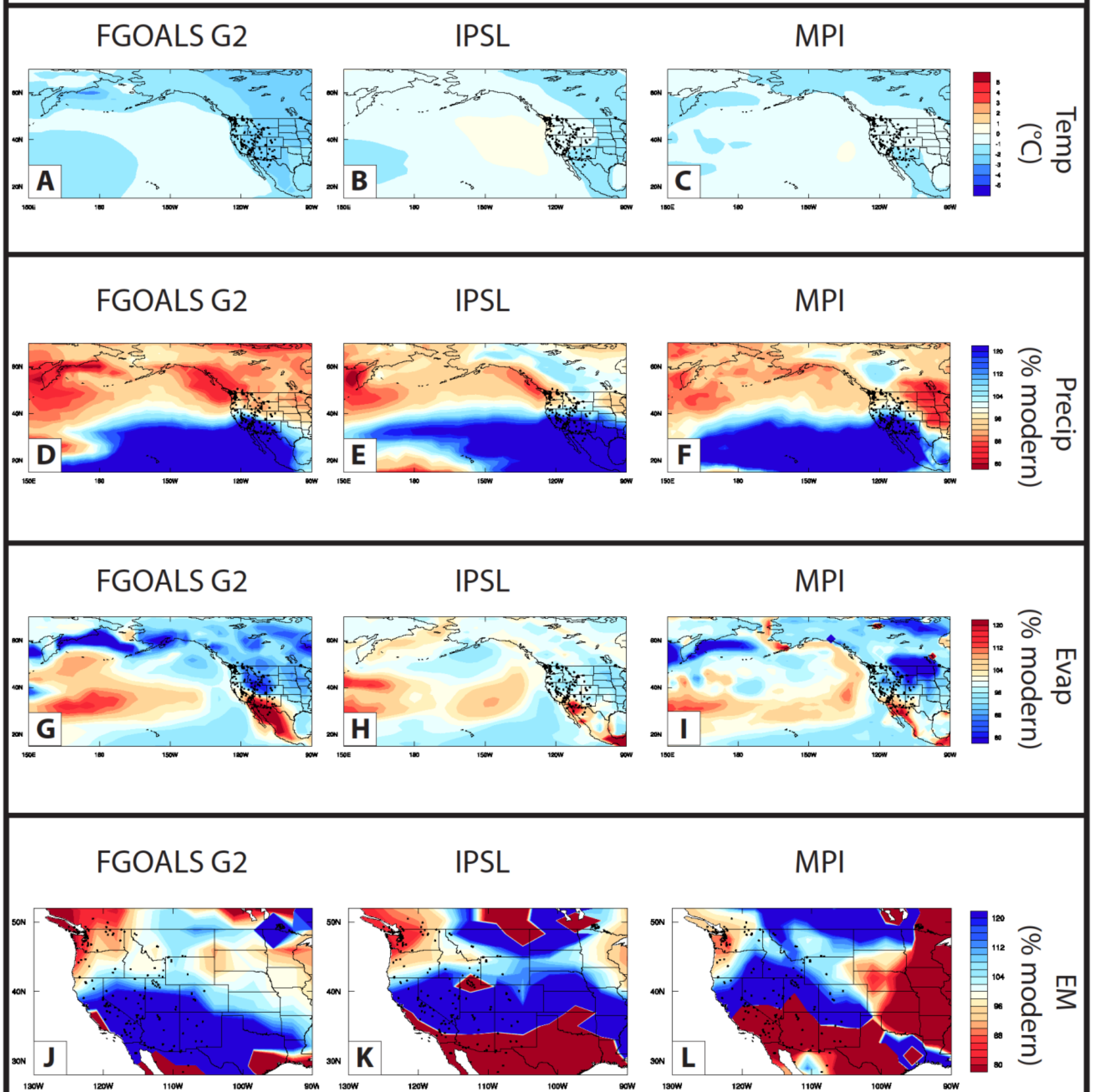

Figure 11: Mid-Holocene spring temperature anomalies (DEGREES C, A-C), precipitation anomalies (% modern, D-F), evaporation anomalies (% modern, G-I), and effective moisture anomalies (% modern, J-L) for FGOALS G2 (A,D,G,J), IPSL (B,E,H,K), and MPI (C,F,I,L).

Figure 12: Summer (JJA) Variables for Top Performing Models

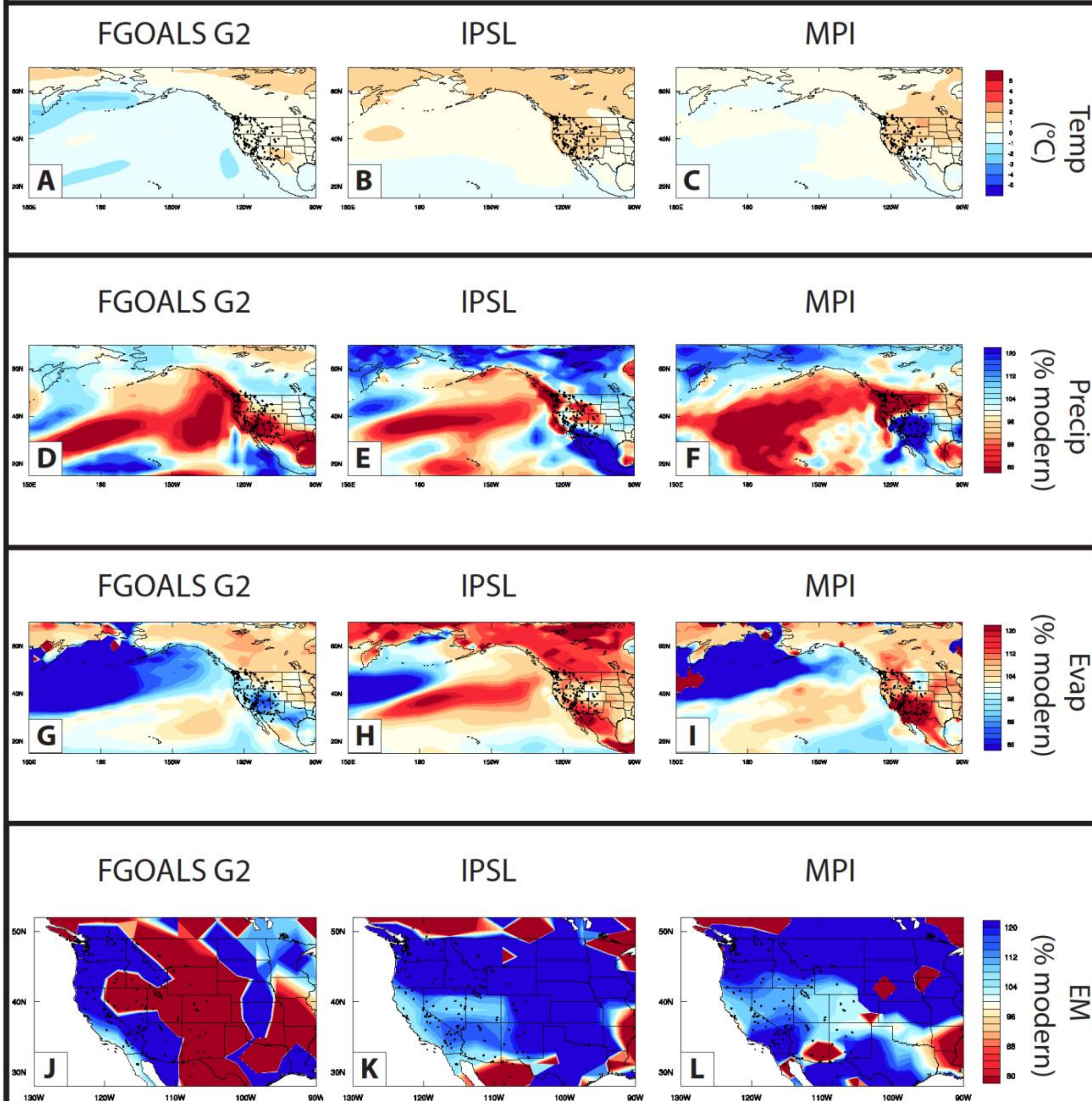

Figure 12: Mid-Holocene summer temperature anomalies (DEGREES C, A-C), precipitation anomalies (% modern, D-F), evaporation anomalies (% modern, G-I), and effective moisture anomalies (% modern, J-L) for FGOALS G2 (A,D,G,J), IPSL (B,E,H,K), and MPI (C,F,I,L).

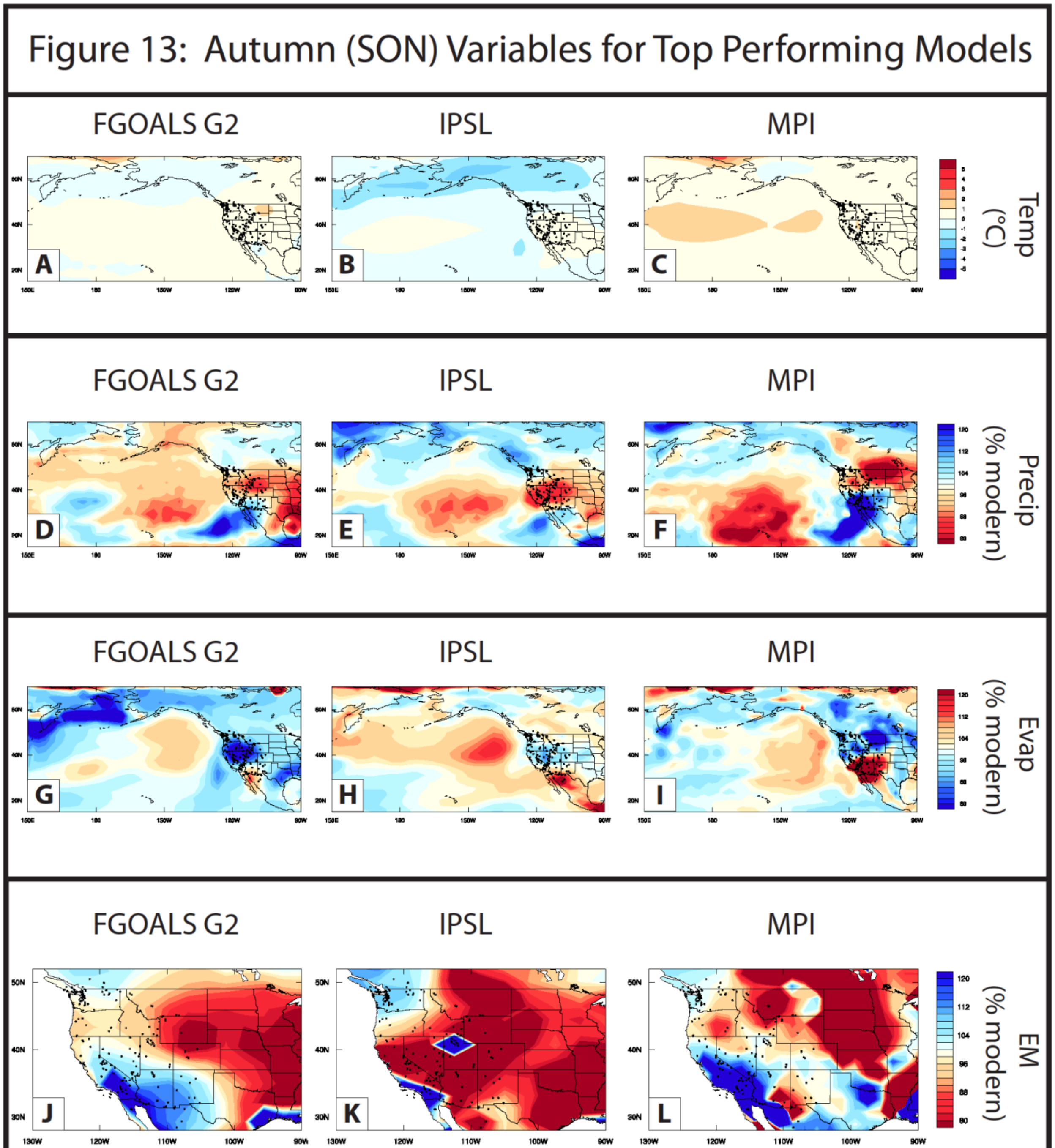

Figure 13: Mid-Holocene autumn temperature anomalies (DEGREES C, A-C), precipitation anomalies (% modern, D-F), evaporation anomalies (% modern, G-I), and effective moisture anomalies (% modern, J-L) for FGOALS G2 (A,D,G,J), IPSL (B,E,H,K), and MPI (C,F,I,L).

ANNUAL SURFACE WIND AND WINTER 250MBAR WIND PATTERNS

The models that show the best agreement with the proxy network (FGOALS G2, IPSL, and MPI) display a distinct boundary between stronger annual westerly winds north of 45°N and weaker annual westerly winds between 30-45°N during the mid-Holocene (Figure 14a-c), though these annual anomalies are small (+/- 1m/s). All other models either do not have this boundary, or it is shifted to a different latitude. Additionally, the center of the North Pacific High (NPH) in FGOALS G2, IPSL, and MPI is exclusively characterized by weaker annual westerly winds, whereas other models have areas of stronger annual westerly winds over the NPH (Figure 14d-f).

Winter 250mbar wind vector anomalies in FGOALS G2, MPI, and CSIRO 312 all show stronger than modern zonal winds in the northeast Pacific offshore of Canada and weaker than modern zonal winds offshore of southern California (Figure 15a-c). Additionally, FGOALS G2, MPI, and CSIRO 312 show stronger than modern poleward winds over the Pacific Ocean and stronger than modern equatorward flow along the U.S. West Coast (Figure 15d-f). These wind anomalies coincide with areas of higher than modern sea level pressure and form an anticyclonic anomaly centered between 150°W-130°W, offshore of northern California and the Pacific Northwest (Figure 16a,c,e), and. The presence of an anticyclonic anomaly in CSIRO 312 indicates that such wind patterns are not exclusive to models with high K_w values, though the highest scoring models (FGOALS G2 and MPI) have them.

Figure 14: Annual Zonal Wind Anomalies and 6ka Sea Level Pressure

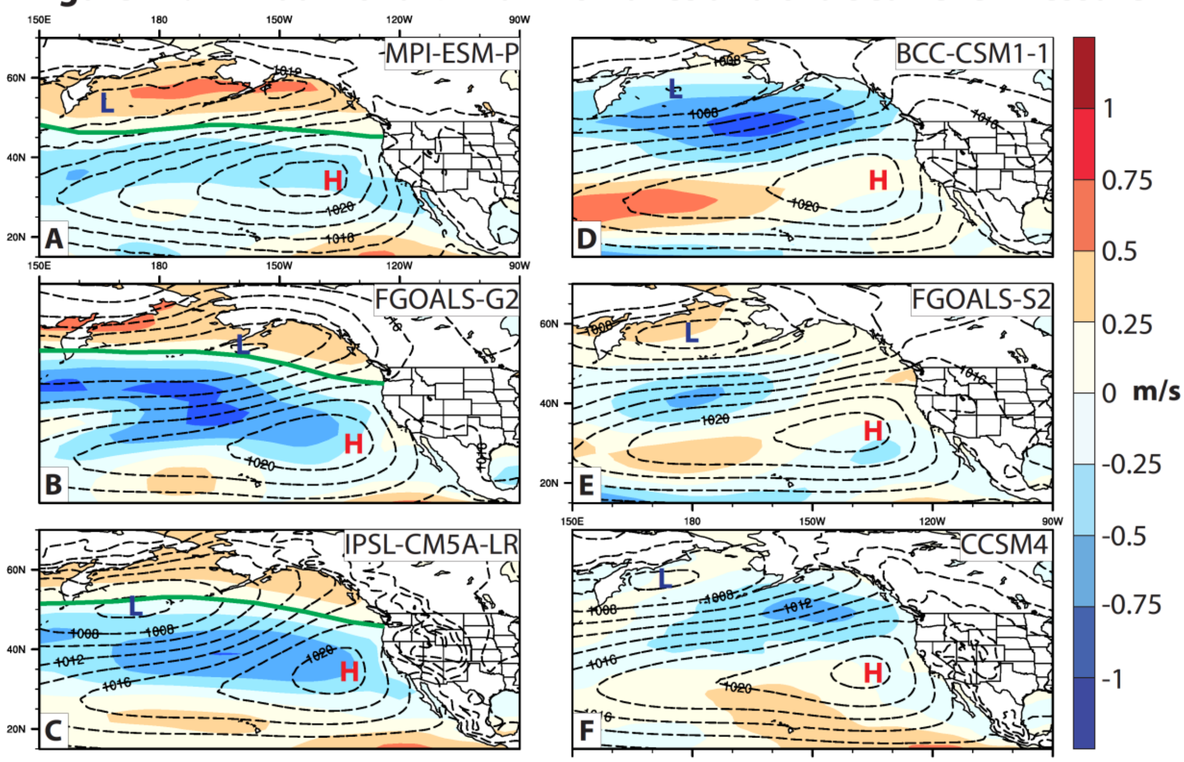

Figure 14: Annual zonal wind anomalies (6ka-modern) for various models. The Aleutian Low and North Pacific High are denoted by blue L's and red H's, respectively, and dashed contours represent 6ka absolute sea level pressure (mbar). In A-C, the green line separates stronger westerly winds in the north and weaker westerly winds to the south in the top three performing models around 45°N. In D-F, this zonal boundary line is not present or displaced. Additionally, A-C show a North Pacific High that entails strictly weaker westerly flow in the top 4mbar contours, whereas D-F show cross-cutting of stronger westerly flow in these strong high pressure zones. The remaining models (not shown here) typically do not have a defined zonal boundary line, and if they do, it extends further south than 45°N.

ANNUAL REGRESSION RESULTS

K_w for annual P shows strong correlation with the NPH strength and westerly position, as well as the pressure difference between the NPH and AL (R^2=0.8908, p=0.0001). The sign of the regression model coefficients indicates K_w for annual P is higher when the NPH is shifted to the west and has higher absolute sea level pressure, and the pressure difference between the NPH and AL is decreased. This suggests that a weaker pressure contrast and higher sea level pressure at both the NPH and AL exert a strong influence on precipitation patterns in western North America.

K_w for annual EM shows slightly weaker correlation with atmospheric pressure variables (R^2=0.8162, p=0.001) than K_w for annual P. The best regression model of EM K_w has two variables that are significant at the 95% CI (NPH and AL sea level pressure). This model's coefficients indicate that EM K_w is highest when the NPH is west shifted (not significant at 95% CI) with lower than modern sea level pressure, and the AL has higher than modern sea level pressure, resulting in an overall decreased pressure difference.

Figure 15: 250mbar Winter (DJF) Zonal and Meridional Wind Anomalies

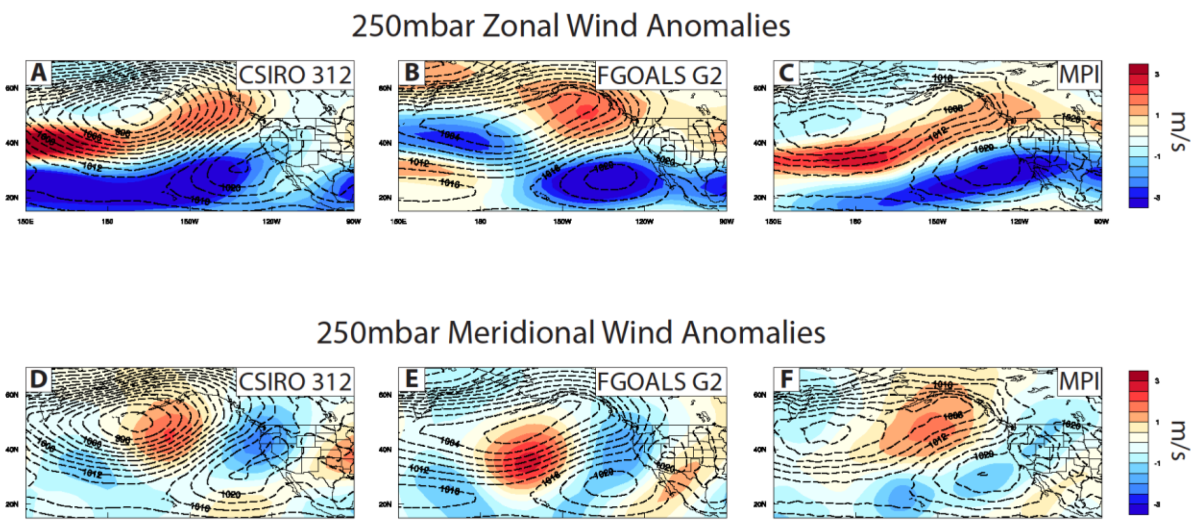

Figure 15: Winter (DJF) 250mbar zonal wind (A-C), meridional wind (D-F), for CSIRO 312 (A,D), FGOALS G2 (B,E), and MPI (C,F). Contours for all figures are mid-Holocene sea level pressure (hPa). Red shades represent stronger eastward and northward flow, respectively.

Figure 16: Winter (DJF) 250mbar Wind, Surface Pressure, and Precipitation Anomalies

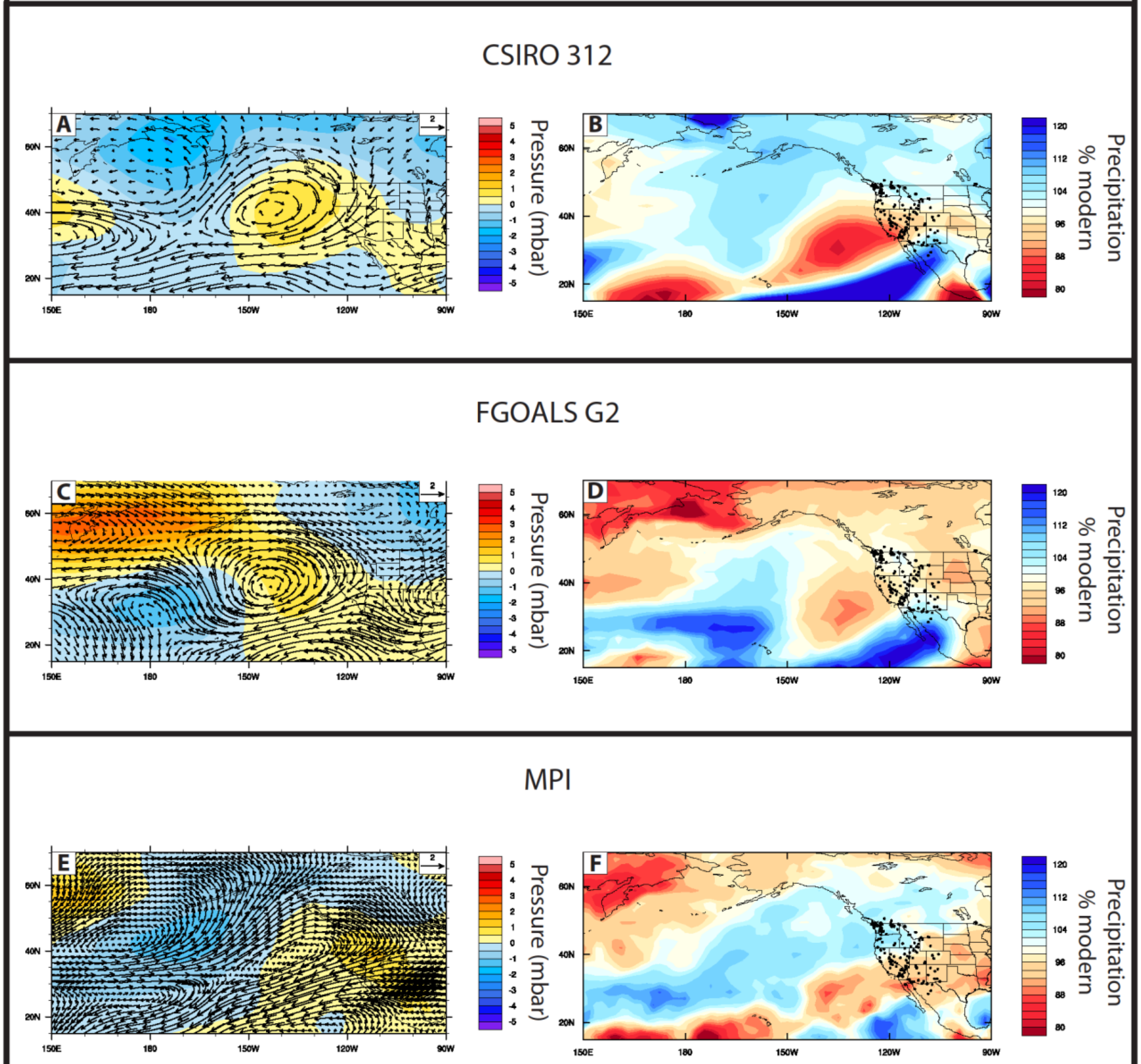

Figure 16: 250mbar wind anomalies (vectors; A,C,E), sea level pressure anomalies (colors; A,C,E), and precipitation anomalies (B,D,F) for the mid-Holocene relative modern. A,C, and E show anticyclonic wind anomalies centered over an area of higher than modern sea level pressure offshore of the Pacific Northwest. B,D, and F show significantly reduced precipitation over California during the winter season.

2013 ANNUAL PRECIPITATION VS. MID-HOLOCENE ANNUAL PRECIPITATION

Compared with the K_w values for PMIP3 model agreement, the model-proxy agreement for the observed 2013 P anomalies from the PRISM dataset is the third highest K_w ($K_w = 0.172$ at the 5-6% threshold). The greatest disagreement between the 2013 P anomalies and the proxy network occurs in the southern Great Basin, Desert Southwest, and Rocky Mountains (Figure 17). Annual precipitation anomalies for 2013 show strong agreement with the mid-Holocene proxy network in the Pacific Northwest and California (29/30 sites in agreement). Thus, although the overall K_w value is not high, there is near perfect agreement when comparing the mid-Holocene proxy record to precipitation anomalies from the 2013 drought at sites where the majority of annual precipitation occurs as winter precipitation from the westerly storm track.

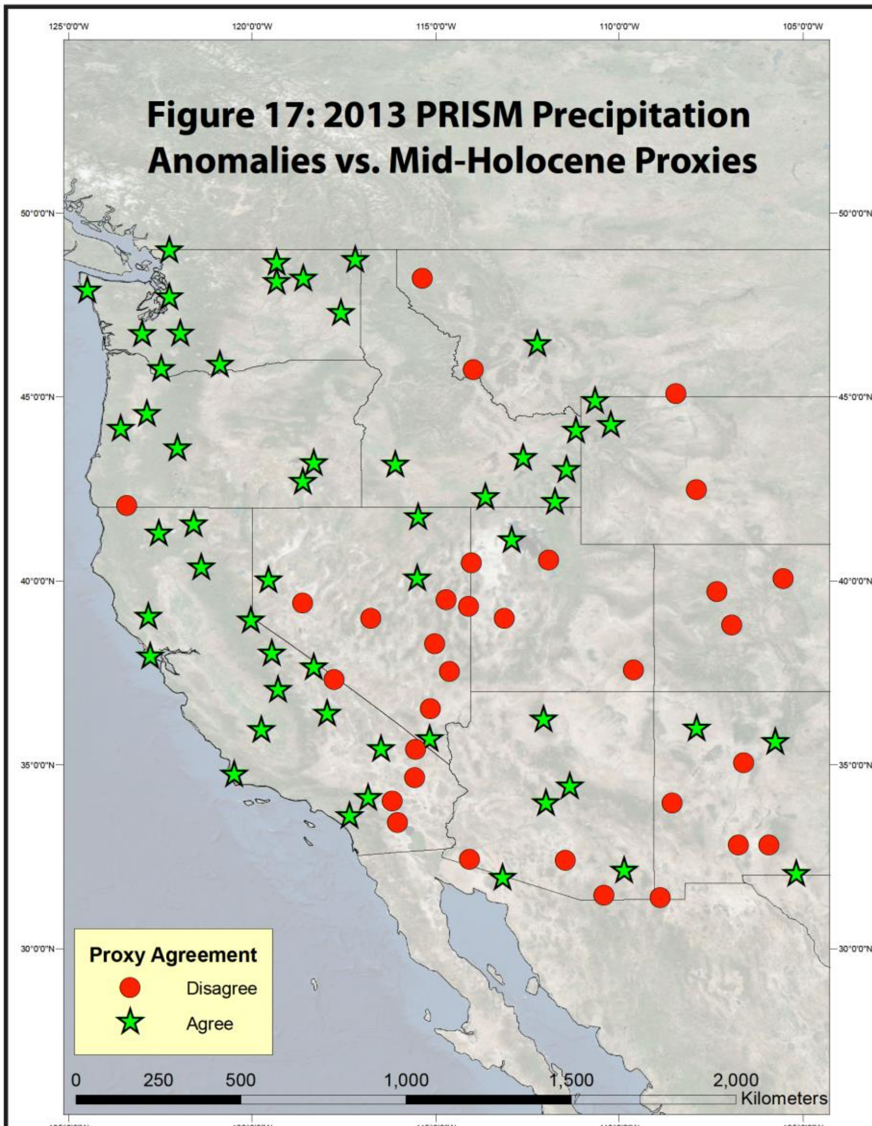

Figure 17: Observed annual precipitation anomalies from 2013 compared with the mid-Holocene proxy network. There is strong agreement between observed 2013 precipitation and the mid-Holocene proxies in the Pacific Northwest, California, northern Great Basin, and northern Rockies.

DISCUSSION

Previous analysis of PMIP3 model simulations of mid-Holocene and Last Glacial Maximum climates indicates that models are generally capable of capturing large-scale features of paleoclimate, such as the North American Monsoon. However, the ability of models to predict the proper magnitude of change, especially on a regional basis, is still an area in need of improvement (Harrison et al 2015). This study, however, suggests that even the sign of change is poorly represented and inconsistent among the PMIP3 simulations of mid-Holocene hydroclimate in western North America, although some models perform notably better than others.

Regional climate models (RCMs) also show disagreement between moisture-sensitive proxy records and simulated mid-Holocene effective moisture (EM) in western North America (Diffenbaugh and Sloan 2004), with RCMs indicating wetter than modern conditions over northern California and southwestern Oregon and proxy records indicating drier than modern conditions. The same model-proxy disagreement is clearly shown in nine of the twelve PMIP3 global climate models (GCMs) considered here (Figure 8b). Of these twelve PMIP3 models, FGOALS G2 and MPI show the best agreement with the proxy network for the mid-Holocene in western North America based on precipitation K_w values. In particular, both models display negative annual precipitation anomalies in the Pacific Northwest and northern Rockies, in agreement with proxies that indicate drier mid-Holocene conditions (Figure 18a and 18d). FGOALS G2, IPSL, and MPI show good agreement with the proxy network for EM, stemming from the prediction of reduced effective moisture in the Pacific Northwest and Northern Rockies (Figure 9a). Most of the PMIP3 models investigated here are producing some combination of too much precipitation and not enough evaporation in the northern study area and thus do not reflect the increased aridity recorded by the proxy network. However, each of the three models that show good agreement in the Pacific Northwest achieves reduced annual EM through slightly different combinations of change in precipitation and evaporation. For example, MPI combines decreased precipitation and increased evaporation in the Pacific Northwest, resulting in overall drier conditions during the mid-Holocene (Figure 18a-c) whereas FGOALS G2 predicts decreased evaporation and a larger decrease in precipitation to compensate (Figure 18d-f). Importantly, the K_w values for EM are consistently higher in FGOALS G2, IPSL, and MPI than those for P, indicating a larger number of proxy sites are accurately represented by moisture balance rather than precipitation alone.

Outside of the Pacific Northwest, several areas of disagreement persist across all models. For example, all models fail to predict EM in the Sierra Nevada and northern Arizona and New Mexico (Figure 9), where proxies indicate drier than modern conditions. FGOALS G2, IPSL, and MPI show excellent agreement at the U.S.-Mexico border where proxies predict wetter mid-Holocene conditions. These models, however, show poor agreement north of the border in the southwestern US where proxies predict drier conditions (Figure 9a). This contrast results from modeled wet conditions in Arizona and New Mexico, suggesting that the models simulate a more expanded mid-Holocene North American Monsoon than is indicated by the proxy record. This may result from relatively coarse resolution topography at the GCM scale (Figure 19), which would lead to the stronger monsoon being able to penetrate further northward because it is not being blocked by orographic barriers.

Figure 18: Annual Moisture-Related Variable Anomalies (% modern)

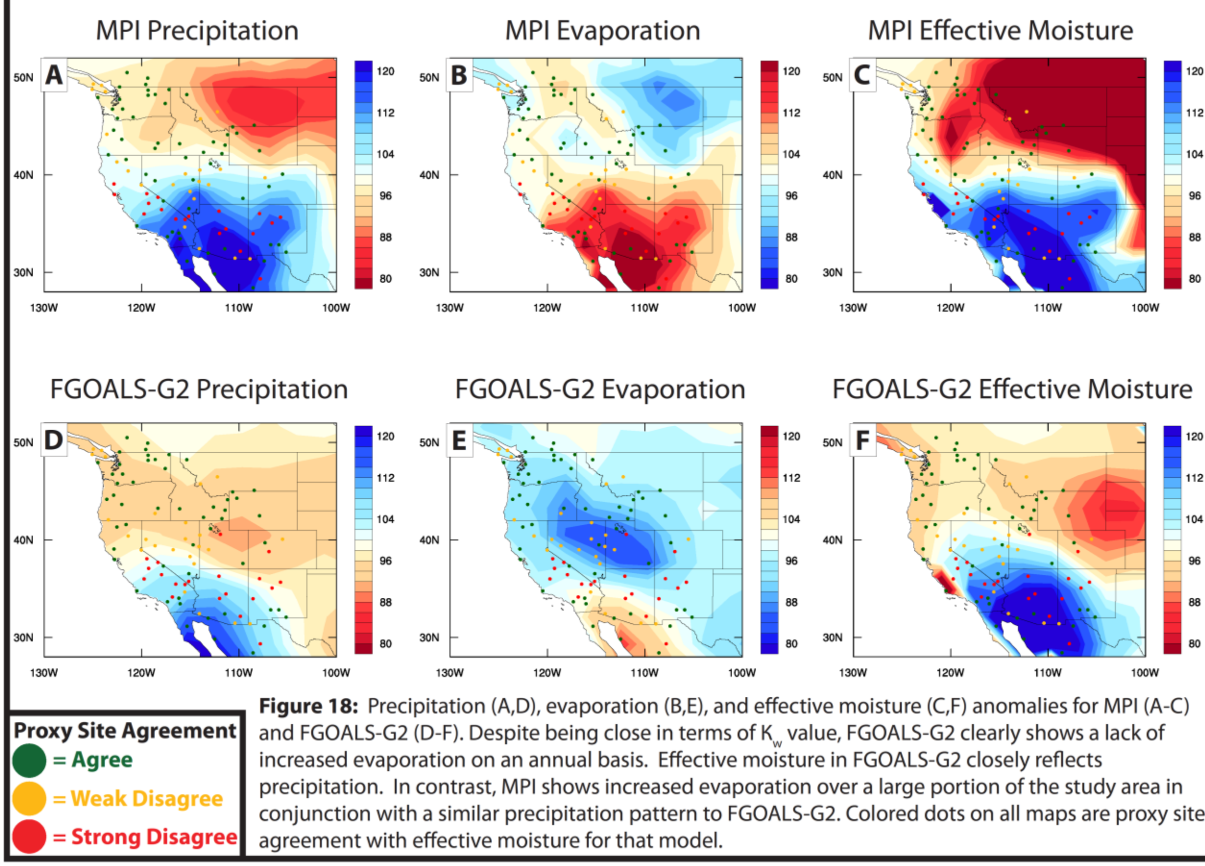

Figure 18: Precipitation (A,D), evaporation (B,E), and effective moisture (C,F) anomalies for MPI (A-C) and FGOALS-G2 (D-F). Despite being close in terms of K_w value, FGOALS-G2 clearly shows a lack of increased evaporation on an annual basis. Effective moisture in FGOALS-G2 closely reflects precipitation. In contrast, MPI shows increased evaporation over a large portion of the study area in conjunction with a similar precipitation pattern to FGOALS-G2. Colored dots on all maps are proxy site agreement with effective moisture for that model.

One potential contributing factor to the model-proxy mismatch might be the short duration of model runs. The models used in this study were run for differing amounts of time (Table 4), and only five models are run long enough (200+ years) to capture multiple phases of the Pacific Decadal Oscillation (PDO). The PDO is essentially a lower frequency and lower magnitude phase of the El Niño-Southern Oscillation (ENSO) and acts on timescales ranging from 20-70 years (Minobe 1999). For the western U.S., cool PDO phases lead to drier conditions in the southern half of the study area and wetter conditions in the Pacific Northwest, while warm phases result in a wetter southern study area and drier Pacific Northwest (Wise 2010). The phase of the PDO also has profound impacts on the magnitude of ENSO events, serving to amplify El Niño events during positive (warm) PDO phases and dampen El Niño events during negative (cool) PDO phases (Wise 2010). Given that a single phase of the PDO can last up to 70 years (Minobe 1999), longer runs of all PMIP3 models to allow for multiple PDO cycles would mitigate potential bias against a particular phase of the PDO and may improve agreement with the proxies. For example, if a simulation is dominated by a cool phase PDO, the Pacific Northwest would be wetter than average and the southern portion of the study area (California, especially) would be drier than average. The cool phase PDO could potentially raise P in the Pacific Northwest and reduce model-proxy agreement there, and at the same time, reduce P in California and increase model-proxy agreement in that region. However, in this analysis, neither P nor EM Kw values correlate strongly with model run time, and thus it is unclear if bias toward a single phase of the PDO influenced model results.

Figure 19: Model Topography

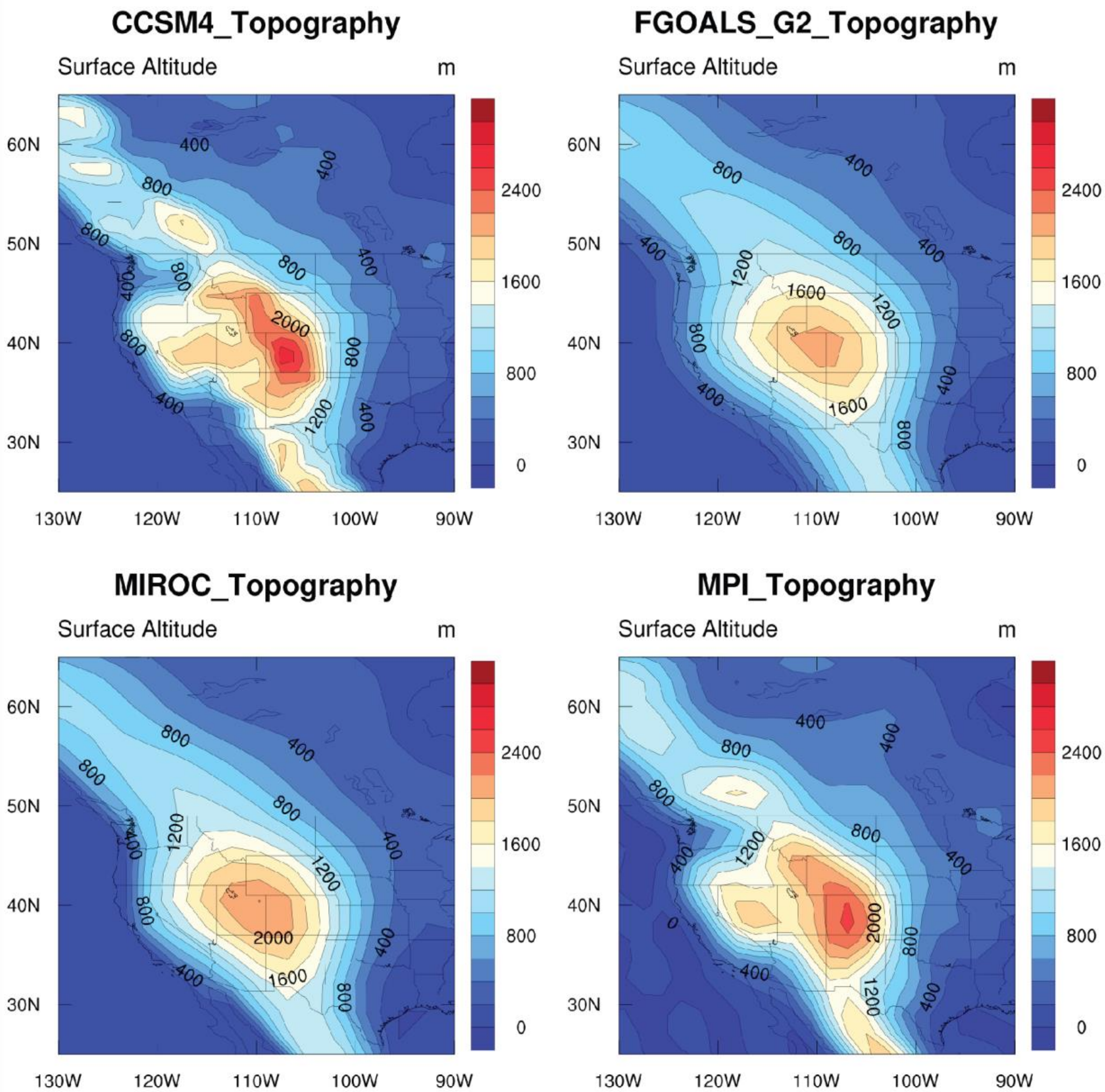

Figure 19: Model topography for four of the PMIP3 models. CCSM4 and MPI extend higher elevation mountain ranges from the Colorado Plateau into northwestern Mexico, while FGOALS G2 and MIROC have relatively shorter mountains in the same area. The variation in topography, in addition to the coarse resolution incorporated into GCM simulations may cause discrepencies in spatial moisture patterns between models and observed precipitation.

Despite differences between models, the models that show the best agreement with the proxy network for P (FGOALS G2 and MPI) and EM (FGOALS G2, IPSL, and MPI) have some similar characteristics. Each of these three models shows positive annual westerly surface wind anomalies north of 45°N and negative westerly surface wind anomalies between 30-45°N at 6ka (Figure 14a-c) indicating northward shifted zonal winds relative to modern. Multivariate results indicate that stronger K_w P agreement corresponds with a strengthened and west-shifted NPH and a weaker contrast between the NPH and AL. The regression models for K_w EM do not have correlations as strong as K_w P, but still indicate that a weaker contrast between the NPH and AL plays a strong role in EM spatial patterns. The weaker correlation for K_w EM likely results from the influence of other factors, such as insolation-driven temperature enhancing evaporation potential. It is clear that changes in large-scale pressure system dynamics in the Pacific and changes in wind strength correspond to changes in spatial patterns of precipitation in the West, and changes in evapotranspiration seem to improve the model-proxy agreement based on higher K_w EM scores than K_w P scores for FGOALS G2, IPSL, and MPI. However, there are consistent problem areas even for the best scoring models, such as California and the Desert Southwest north of the U.S.-Mexico border (Figure 9a).

Precipitation patterns for 2013 show better agreement with the proxy network than all PMIP3 simulations of mid-Holocene precipitation with the exception of FGOALS G2 and MPI. During the mid-Holocene, proxy records indicate wetter than modern conditions in the Desert Southwest (Figure 3), and these changes were driven by a stronger than modern monsoon season due to increased summer insolation (Metcalfe et al 2015). Today, the North American Monsoon is not as strong as the mid-Holocene, and therefore, would not be expected to show wetter conditions in the Desert Southwest. Indeed, the 2013 precipitation anomalies and the 6ka proxy network show most disagreement in the Desert Southwest and southern Great Basin, while sites in the Pacific Northwest and California show almost perfect agreement (29/30 sites; Figure 17). Today, the majority of annual precipitation for the Pacific Northwest and California comes from the westerly storm track during the winter season. During the 2013 drought year, a combination of 1) weaker westerly winds over the Pacific south of ~50°N; 2) stronger westerly winds over Alaska; 3) stronger equatorward flow over the Pacific Northwest; and 4) stronger poleward flow on the western flank of the pressure ridge, all acted in tandem to deflect precipitation north of the U.S. west coast (see Figure 2.1 in Swain et al., 2014).

The mid-Holocene winter season is characterized in the CSIRO 312, FGOALS G2, and MPI simulations by a combination of greater than modern sea level pressure anomalies and 250mbar anticyclonic wind vector anomalies offshore of the Pacific Northwest around 140°W (Figure 16a,c,e). The presence of anticyclonic winter wind anomalies and higher sea level pressure offshore of the U.S. west coast are strikingly similar to conditions seen in the 2013 drought year (Seager et al 2014; Swain et al 2014). However, the latitude of the wind anomalies is further south-shifted in the mid-Holocene simulations than what is observed in the 2013 drought year. Additionally, the configuration of anticyclonic wind anomalies for MPI is a more elongated southwest-northeast trending pattern (Figure 16e), while the modern pressure ridge is more symmetrical. This similarity between the 2013 annual atmospheric configuration and simulated configuration during mid-Holocene winters suggests that anticyclonic wind anomalies and higher sea level pressure offshore of western North America are important features that lead to dry conditions in California in both cases. Interestingly, the 2013 drought matches the annual precipitation pattern seen in the mid-Holocene proxy network perfectly in California (Figure 17), while mid-Holocene models consistently fail in this region on an annual basis (Figure 8). However, the winter season in the CSIRO 312, FGOALS G2, and MPI mid-Holocene simulations displays similar atmospheric conditions to the 2013 drought year, and these models successfully simulate drier conditions in California and parts of the Pacific Northwest during the winter season (Figure 16). CSIRO 312 shows poor agreement with the proxy network for annual

P despite showing anticyclonic anomalies during mid-Holocene winters, and this results from higher than modern P in the spring and autumn seasons over most of the study area. The strong agreement between mid-Holocene proxies and 2013 precipitation anomalies indicates that large scale atmospheric patterns which controlled precipitation in 2013 are likely a key component of mid-Holocene aridity, although most models do not produce wind and pressure anomalies consistent with those seen in 2013. Nevertheless, the strong agreement between the mid-Holocene proxy network and 2013 precipitation anomalies in the Pacific Northwest and California provides evidence that the mid-Holocene may be a good comparative case study for modern droughts, and conversely, the modern drought may provide insight into atmospheric drivers of climate during the arid mid-Holocene.

CONCLUSIONS

I have compiled an updated network of moisture-sensitive proxy records for western North America during the mid-Holocene. The proxy network indicates drier than modern conditions in the Pacific Northwest, California, northern Great Basin, and northern Rocky Mountains, while climate was wetter than modern in the Desert Southwest, parts of the southern Great Basin, and the Colorado Plateau due to a stronger North American Monsoon. Using the K_w statistic to measure model-proxy agreement, I found that effective moisture (P-E) shows better model-proxy agreement than precipitation alone. I have also established that the models that show the closest agreement with the proxy network capture arid conditions in the Pacific Northwest during the mid-Holocene, though there are multiple combinations of evaporation and precipitation changes that lead to successful agreement with the proxy network. In the southern portion of the study area, topographic complexity may not be adequately captured by GCMs, leading to most models simulating much wetter conditions north of the U.S.-Mexico border than is evident in the proxy record, possibly resulting from monsoonal moisture penetrating too far northward in the models. Of the twelve models examined here, I find that FGOALS G2, IPSL, and MPI best reflect mid-Holocene EM conditions in the western U.S. The mechanisms driving more arid conditions over much of the West include weaker annual westerly winds across the Pacific Ocean from 30-45°N, the development of anticyclonic 250mbar wind anomalies offshore of the Pacific Northwest during the winter, and increased evaporation rates over much of the study area, especially during the summer. The 2013 drought year shows similar annual atmospheric configuration to that observed in the mid-Holocene simulations. In fact, proxy records from regions where precipitation is dominated by winter westerly storms more closely match the 2013 drought pattern than the precipitation patterns simulated in mid-Holocene model simulations. The similarities between precipitation patterns seen in paleodroughts and those seen today suggests that atmospheric conditions of modern droughts must be better represented in climate models in order to properly recreate drought conditions of the mid-Holocene. Comparison of the 2013 drought year, mid-Holocene moisture proxies, and GCM simulations for 6ka reveal that although key differences exist between modern and past droughts, the mid-Holocene likely provides a good case study for comparison to current conditions in California and the Pacific Northwest.

REFERENCES

Adam, D.P., 1988, Palynology of Two Upper Quaternary Cores from Clear Lake, Lake County, California: USGS Professional Paper 1363, Washington D.C.

Anderson, R.S., 1990, Holocene Forest Development and Paleoclimates within the Central Sierra Nevada, California: Journal of Ecology, vol 78, no 2, pp. 470-489.

Anderson, L., 2012, Rocky Mountain hydroclimate: Holocene variability and the role of insolation, ENSO, and the North American Monsoon: Global and Planetary Change 92-93, pp. 198-208.

Anderson, R.S., and Van Devender, T.R., 1991, Comparison of pollen and macrofossils in packrat (Neotoma) middens: A chronological sequence from the Waterman Mountains of southern Arizona, U.S.A.: Review of Paelaeobotany and Palynology, 68, pp. 1-28.

Anderson, R.S., and Van Devender, T.R., 1995, Vegetation history and paleoclimates of the coastal lowlands of Sonora, Mexico – pollen records from packrat middens: Journal of Arid Environments, 30, pp. 295-306.

Anderson, R.S., Ejarque, A., Brown, P.M., and Hallett, D.J., 2013, Holocene and historical vegetation change and fire history on the north-central coast of California, USA: The Holocene, 23(12), 1797-1810.

Anderson, R.S., Ejarque, Rice, J., Smith, S.J., and Lebow, C.G., 2015, Historic and Holocene environmental change in the San Antonio Creek Basin, mid-coastal California: Quaternary Research, 83, pp. 273-286.

Anderson, R.S., 1993, A 35,000 year vegetation and climate history from Potato Lake, Mongollon Rim, Arizona: Quaternary Research, 40, pp. 351-359.

Asmerom, Y., Polyak, V.J., and Burns, S.J., 2010, Variable winter moisture in the southwestern United States linked to rapid glacial climate shifts: Nat. Geosci. Lett., 3, pp. 114-117.

Bacon, S.N., Burke, R.M., Pezzopane, S.K., and Jayko, A.S., 2006, Last glacial maximum and Holocene lake levels of Owens Lake, eastern California, USA: Quat. Sci. Rev., 25, pp. 1264-1282.

Baker, R.G., 1976, Late Quaternary Vegetation History of the Yellowstone Basin, Wyoming: USGS Professional Paper 729-E, Washington D.C.

Barnosky, C.W., 1981, A record of late quaternary vegetation from Davis Lake, southern Puget lowland, Washington. Quat. Res., 16, pp.221-239.

Barnosky, C.W., 1985, Late quaternary vegetation near Battle Ground Lake, southern Puget Trough, Washington: Geological Society of America Bulletin 96, pp. 263-271.

Bartoń, K., MuMIn: Multi-Model Inferences, R Package (R Foundation for Statistical Computing, 2014); http://cran.r-project.org/web/packages/MuMIn/MuMIn.pdf.

Beiswenger, J.M., 1991, Late quaternary vegetational history of Grays Lake, Idaho: Ecological Monographs, 61, pp. 165-182.
Betancourt, J.L., and Davis, O.K., 1984, Packrat middens from Canyon de Chelley, northeastern Arizona: Paleoecological and archaeological indications: Quat. Res., 21, pp. 56-64.

Benson, L. Kashgarian, M., Rye, R., Lund, S.,; Paillet, F., Smoot, J., Kester, C., Mensing, S., Meko, D., and Landström, S., 2002, Holocene multidecadal and multicentennial droughts affecting Northern California and Nevada: USGS Staff -- Published Research, Paper 365.

Betancourt, J.L., and Van Devender, T.R., 1981, Holocene vegetation in Chaco Canyon, New Mexico: Science, 214, pp. 656-658.

Bird, B.W., Kirby, M.E., 2006. An alpine lacustrine record of early Holocene North American Monsoon dynamics from Dry Lake, southern California (USA): J. Paleolimnol, 35, pp. 179-192.

Bloom, A.M., 2006, A paleolimnological investigation of climatic and hydrological conditions during the late Pleistocene and Holocene in the Sierra Nevada, California, USA: Ph.D. Dissertation. University of Utah, Department of Geography, Salt Lake City.

Braconnot, P., Harrison, S.P., Kageyama, M., Bartlein, P.J., Masson-Delmotte, V., Abe-Ouchi, A., Otto-Bliesner, B., and Zhao, Y., 2012, Evaluation of climate models using palaeoclimatic data: *Nat. Clim. Change*, 2, pp. 417-424.

Briles, C.E., Whitlock, C., and Bartlein, P.J., 2005, Postglacial vegetation, fire, and climate history of the Siskiyou Mountains, Oregon, USA: Quat. Res., 64, pp. 44-56.

Brown, K.J., and Hebda, R.J., 2003, Coastal rainforest connections disclosed through a Late Quaternary vegetation, climate, and fire history investigation from the Mountain Hemlock Zone on southern Vancouver Island, British Columbia, Canada: Review of Palaeobotany and Palynology, 123, pp. 247-269.

Brown, K.J., Fitton, R.J., Schoups, G., Allen, G.B., Wahl, K.A., and Hebda, R.J., 2006, Holocene precipitation in the coastal temperate rainforest complex of southern British Columbia, Canada: Qat. Sci. Rev., 25, pp. 2762-2779.

Brunelle, A., and Anderson, R.S., 2003, Sedimentary charcoal as an indicator of late-Holocene drought in the Sierra Nevada, California, and its relevance to the future: The Holocene, 13, pp 21-28.

Castiglia, P.J., Fawcett, P.J., 2006, Large Holocene lakes and climate change in the Chihuahuan Desert: Geology, 34, pp. 113-116.

Cohen, J., 1968, Weighed kappa: Nominal scale agreement with provision for scaled disagreement or partial credit". *Psychol. Bull.* 70 (4): 213–220.doi:10.1037/h0026256.

Cole, K.L., 1981, Late Quaternary Environments in the Eastern Grand Canyon: Vegetational Gradients Over the Last 25,000 Years: PhD Thesis, University of Arizona.

Davis, Owen K., 1999, Pollen Analysis of a Late-Glacial and Holocene Sediment Core from Mono Lake, Mono County, California: Quat. Res., 52, pp. 243-249.

Davis, O.K., 1999, Pollen analysis of Tulare Lake, California: Great Basin-like vegetation in Central Califronia during the full-glacial and early Holocene: Review of Palaeobotany and Palynology, 107, pp. 249-257.

Davis, O.K., and Shafer, D.S., 1992, A Holocene climatic record for the Sonoran Desert from the pollen analysis of Montezuma Well, Arizona, USA: Palaeogeogr., Palaeoclimatol., Palaeoecol, 92, pp. 107-119.

Davis, O.K., Anderson, R.S., Fall, P.L., O'Rourke, M.K., and Thompson, R.S., 1985, Palynological evidence for early Holocene aridity in the southern Sierra Nevada, California: Quat. Res., 24, pp. 322-332.

Diffenbaugh, N.S., and Sloan, L.C., 2004, Mid-Holocene Orbital Forcing of Regional-Scale Climate: A Case Study of Western North America Using a High-Resolution RCM: *American Meteorological Society*, p. 2927-2937.

Diffenbaugh, N.S., Bell, J.L., and Sloan, L.C., 2006, Simulated changes in extreme temperature and precipitation events at 6 ka: Palaeogeogr. Palaeocl., 236, ppp. 151-168.

Diffenbaugh, N.S., Swain, D.L., and Touma, D., 2015, Anthropogenic warming has increased drought risk in California: *Proc. Natl. Acad. Sci.*, 112 (13), p. 3913-3936.

DiNezio, P.N., and Tierney, J.E., 2013, The effect of sea level on glacial Indo-Pacific climate: *Nat. Geosci*., 6, p. 485-491.

Dunwiddie, P.W., 1986, A 6000-Year Record of Forest History on Mount Rainier, Washington: Ecology, 67, pp. 58-68.

Ersek, V., Clar, P.U., Mix, A.C., Cheng, H., and Edwards, R.L., 2012, Holocene winter climate variability in mid-latitude western North America: Nature Communications, DOI: 10.1038/ncomms2222.

Fall, P.L., 1988, Vegetation Dynamics in the Southern Rocky Mountains: Late Pleistocene and Holocene Timberline Fluctuations: PhD Thesis, University of Arizona, Tucson.

Grayson, D.K., 2000, Mammalian responses to Middle Holocene climatic change in the Great Basin of the western United States: Journal of Biogeography, 27, pp. 181-192.

Griffen, D., and Anchukaitis, K.J., 2014, How unusual is the 2012-2014 California drought?: *Geophys. Res. Lett.,* 41, p. 9017-9023.

Hall, W.E., Van Devender, T.R., and Olson, C.A., 1988, Late Quaternary Arthropod Remains from Sonoran Desert Packrat Middens, Southwestern Arizona and Northwestern Sonora: Quat. Res., 29, pp. 277-293.

Hansen, B.S., and Easterbrook, D.J., 1974, Stratigraphy and palynology of late Quaternary sediments in the Puget lowland, Washington: Geological Society of America Bulletin, 85, pp. 587-602.

Harrison, S.P., Bartlein, P.J., Brewer, S., Prentice, L.C., Boyd, M., Hessler, I., Holmgren, K., Izumi, K., and Willis, K., 2014: Climate model benchmarking with glacial and mid-Holocene climates: *Clim. Dyn.*, 43, p. 671-688.

Holmgren, C.A., Betancourt, J.L., and Rylander, K.A, 2006, A 36,000-yr vegetation history from the Peloncillo Mountains, southeastern Arizona: Palaeogeogr., Palaeoclimatol., Palaeoecol., 240, pp. 405-422.

Holmgren, C.A., Betancourt, J.L., and Rylander, K.A., 2009, A long-term vegetation history of the Mojave-Colorado Desert ecotone at Joshua Tree National Park: J. Quat. Sci., 25, pp. 222-236.

Holmgren, C.A., Betancourt, J.L., and Rylander, K.A., 2011, Vegetation history along the eastern desert escarpment of the Sierra San Pedro Martir, Baja California, Mexico: Quat. Res., 75, pp. 647-657.

Huesser, C.J., 1973, Environmental sequence following the Fraser advance of the Juan de Fuca lobe, Washington: Quat. Res., 3, pp. 284-304.

Huesser, C.J., 1974, Quaternary vegetation, climate, and glaciation of the Hoh River Valley, Washington: Geological Society of America Bulletin, 85, pp. 1547-1560.

Huesser, C.J., 1977, Quaternary paleoecology of the Pacific slope of Washington: Quat. Res., 8, pp. 282-306.

IPCC, 2014: Climate Change 2014: Synthesis Report. Contribution of Working Groups I, II and III to the Fifth Assessment Report of the Intergovernmental Panel on Climate Change [Core Writing Team, R.K. Pachauri and L.A. Meyer (eds.)]. IPCC, Geneva, Switzerland, 151 pp.

Jennings, S.A., and Elliott-Fisk, D., 1993, Packrat Midden Evidence of Late Quaternary Vegetation Change in the White Mountains, California-Nevada: Quat. Res., 39, pp. 214-221.

Jiménez Moreno, G., Fawcett, P.J., and Anderson, R.S., 2008, Millenial- and centennial-scale vegetation and climate changes during the late Pleistocene and Holocene from northern New Mexico: Quat. Sci. Rev., 27, pp. 1442-1452.

King, T.J., 1976, Late Pleistocene-early Holocene history of coniferous woodlands in the Lucerne Valley region, Mojave Desert, California: Great Basin Naturalist, 36, pp. 227-238.

Kirby, M.E., Lund, S.P., Patterson, W.P., Anderson, M.A., Bird, B.W., Ivanovici, L., Monarrez, P., and Nielsen, S., 2010, A Holocene record of Pacific Decadal Oscillation (PDO)-related hydrologic variability in Southern California (Lake Elsinore, CA): J. Paleolimnol, 44, pp. 819-839.

Kirby, M.E., Zimmerman, S.R.H., Patterson, W.P., and Rivera, J.J., 2012, A 9170-year record of decadal-to-multi-centennial scale pluvial episodes from the coastal Southwest United States: a role for atmospheric rivers?: Quat. Sci. Rev., 46, pp. 57-65.

Kirby, M.E., Knell, E.J., Anderson, W.T., Lachniet, M.S., Palermo, J., Eeg, H., Lucero, R., Murrieta, R., Arevalo, A., Silveria, E., and Hiner, C.A., 2015, Evidence for insolation and Pacific forcing of late glacial through Holocene climate in the Central Mojave Desert (Silver Lake, CA): Quat. Res., 84, pp. 174-186.

Krider, P.R., 1998, Paleoclimatic significance of late Quaternary lacustrine and alluvial stratigraphy, Animas Valley, New Mexico: Quat. Res., 50, pp. 283-289.

Koehler, P.A., Anderson, R.S., and Spaulding, W.G., 2005, Development of vegetation in the Central Mojave Desert of California during the late Quaternary: Palaeogeogr., Palaeoclimatol., Palaeoecol., 215, pp. 297-311.

Kutzbach, J.E., and Ruddiman, W.F., 1993, Climatic Changes in the Western United States since 18,000 yr B.P. In Wright, H.E., Jr., Kutzbackm J.E., Webb, T. III., Ruddiman, W.F., Street-Perrott, F.A., and Bartlein, P.J., editors, *Global climates since the last glacial maximum*, Minneapolis, Minnesota: University of Minnesota Press, 12-23.

Leopold, E.B., Nickmann, R.J., Hedges, J.L., and Ertel, J.R., 1982, Pollen and lignin records of late Quaternary vegetation, Lake Washington: Science, 218, pp. 1305-1307.

Li, H., Xu, X., Ku., T., You, C., Buchheim, H.P., and Peters, R., 2008, Isotopic and geochemical evidence of paleoclimate changes in Salton Basin, California during the past 20 kyrs: 1. $\Delta^{18}O$ and $\delta^{13}C$ records in lake tufa deposits: Palaeogeogr., Palaeoclimatol., Palaeoecol., 109, pp. 193-210.

Lindström, S., 1990, Submerged Tree Stumps as Indicators of Mid-Holocene Aridity in the Lake Tahoe Region: Journal of California and Great Basin Anthropology, 12, pp. 146-157.

Louderback, L.A., and Rhode, D.E., 2009, 15,000 Years of vegetation change in the Bonneville basin: the Blue Lake pollen record: Quat. Sci. Rev., 28, pp. 308-326.

Lowe, D.J., Green, J.D., Northcote, T.G., and Hall, K.J., 1997, Holocene Fluctuations of a Meromictic Lake in Southern British Columbia: Quat. Sci. Rev., 48, pp. 100-113.

Lundeen, Z., Brunelle, A., Burns, S.J., Polyak, V., and Asmerom, Y., 2013, A speleothem record of Holocene paleoclimate from the northern Wasatch Mountains, southeast Idaho, USA: Quaternary International, 310, pp. 83-95.

Lyford, M.E., Betancourt, J.L., and Jackson, S.T., 2002, Holocene Vegetation and Climate History of the Northern Bighorn Basin, Southern Montana: Quat. Sci. Rev., 58, pp. 171-181.

Mack, R.N, Rutter, N.W., Valastro, S., 1978a, Late Quaternary pollen record from the Sanpoil River Valley, Washington: Canadian Journal of Botany, 56, pp. 1642-1650.

Mack, R.N., Rutter, N.W., Valastro, S., and Bryant, V.M., 1978b, Late Quaternary vegetation history at Waits Lake, Colville River Valley, Washington: Botanical Gazetter, 139, pp. 499-506.

Mack, R.N, Rutter, N.W., Valastro, S., 1979, Holocene vegetation history of the Okanogan Valley, Washington: Quat. Res., 12, pp. 212-225.

Mack, R.N, Rutter, N.W., Valastro, S., 1983, Holocene vegetational history of the Kootenai River Valley, Montana: Quat Res., 20, pp. 177-193.

Madsen, D.B., and Currey, D.R., 1979, Late Quaternary glacial and vegetation changes, Little Cottonwood Canyon area, Wasatch Mountains, Utah: Quat. Res., 12, pp. 254-270.

Maher, L.J., Jr., 1972, Absolute pollen diagram of Redrock Lake, Boulder County, Colorado: Quat. Res., 2, 531-553.

Markgraf, V., and Scott, L., 1981, Lower timerline in central Colorado during the past 15,000 yr.: Geology, 9, pp. 231-234.

Markgraf, V., Bradbury, J.P., Forester, R.M., Singh, G., Sternberg, R.S., 1984. San Agustin Plains, New Mexico: age and paleoenvironmental potential reassessed: Quat. Res., 22, pp. 336-343.

Matthewes, R.W., 1973, A palynological study of postglacial vegetation changes in the University Research Forest, southwestern British Columbia: Canadian Journal of Botany, 51, pp. 2085-2103.

Maupin, M.A., Kenny, J.F., Hutson, S.S., Lovelace, J.K., Barber, N.L., and Linsey, K.S., 2014, Estimated use of water in the United States in 2010: U.S. Geological Survey Circular 1405.

McAuliffe, J.R. and Van Devender, T.R., 1998, A 22,000-year record of vegetation and climate change in the north-central Sonoran Desert: Palaeogeogr., Paleoclimatol., Palaeoecol, 141, pp. 253-275.

Mehringer Jr., P.J., Martin, P.S., and Haynes Jr., C.V., 1967, Murray Springs – A mid-post-glacial pollen record from southern Arizona: Am. J. Sci., 265, pp. 786-797.

Menking, K.M. and Anderson, R.Y., 2003, Contributions of La Niña and El Niño to middle Holocene drought and late Holocene moisture in the American Southwest: Geology, 31, pp. 937-940.

Metcalfe, S.E., Barron, J.A., and Davies, S.J., 2015, The Holocene history of the North American Monsoon: “known knowns” and “known unknowns” in understanding its spatial and temporal complexity. *Quat. Sci. Rev.* 120, pp. 1-27.

Minobe, S., 1999, Resonance in bidecadal and pentadecadal climate oscillations over the North Pacific: Role in climatic regime shifts: *Geophys. Res. Lett.*, 26, pp. 855-858.

Mock, C.J., and Brunelle-Daines, A.R., 1999, A modern analogue of western United States summer palaeoclimate at 6000 years before present: Holocene, 9, pp. 541-545.

Mohr, J.A., Whitlock, C., and Skinner, C.N., 2000, Postglacial vegetation and fire history, eastern Klamath Mountains, California, USA: The Holocene, 10, pp. 587-601.

Ortega-Rosas, C.I., Peñalba, M.C., and Guiot, J., 2008, Holocene altitudinal shifts in vegetation belts and environmental changes in the Sierra Madre Occidental, Northwestern Mexico, based on modern and fossil pollen data: Rev. Palaeobot. Palynol., 151, pp. 1-20.

Oster, J.L., Ibarra, D.E., Winnick, M.J., and Maher, K., 2015, Steering of westerly storms over western North America at the Last Glacial Maximum: *Nat. Geosci. Lett.*, DOI: 10.1038/NGEO2365.

Oviatt, C.G., 1988, Late Pleistocene and Holocene lake fluctuations in the Sevier Lake basin, Utah, USA: Journal of Paleolimnology, 1, pp. 9-21.

PRISM Climate Group, Oregon State University, http://prism.oregonstate.edu, created 4 Feb 2004. Accessed 4 Feb 2016.

Reinemann, S.A., Porinchu, D.F., Bloom, A.M., Mark, B.G., and Box, J.E., 2009, A multi-proxy paleolimnological reconstruction of Holocene climate conditions in the Great Basin, United States: Quat. Res., 72, pp. 347-358.

Roy, P.D., Caballero, M., Lozano, R., Ortega, R., Pi., T., Israde, I, and Morton, O., 2010, Geochemical record of Late Quaternary paleoclimate from lacustrine sediments of paleo-lake San Felipe, western Sonora Desert, Mexico: J.S. Am. Earth Sci., 29, pp. 586-596.

Roy, P.D., Quiroz-Jiménez, J.D., Pérez-Cruz, L.L., Lozano-García, S., Metcalfe, S.E., Lozano-Santacruz, R., López-Balbiaux, N., Sánchez-Zavala, J.L., and Romero, F.M., 2013, Late Quaternary paleohydrological conditions in the drylands of northern Mexico: a summer precipitation proxy record of the last 80 cal ka BP: Quat. Sci. Rev., 78, pp. 342-354.

Sea, D.S., and Whitlock, C., 1995, Postglacial Vegetation and Climate of the Cascade Range, Central Oregon: Quat. Res., 43, pp. 370-381.

Seager, R., Hoerling, M., Wang, S.S.H., Lyon, B., Kumar, Arun, M., and Henderson, J.N.N., 2014: Causes and Predictability of the 2011-14 California Drought. Retrieved from NOAA Drought Task Force, http://cpo.noaa.gov/ClimatePrograms/ModelingAnalysisPredictionsandProjections/MAPPTaskForces/DroughtTaskForce1/CaliforniaDrought.aspx.

Spaulding, W.G., 1980, The Presettlement Vegetation of the California Desert: Riverside Desert Planning Staff, California Bureau of Land Management, Riverside.

Smith, S.J., and Anderson, R.S., 1992, Late Wisconsin Paleoecologic Record from Swamp Lake, Yosemite National Park, California: Quat. Res., 38, pp. 91-102.

Spaulding, W.G., 1991, A middle Holocene vegetation record from the Mojave Desert of North America and its paleoclimatic significance: Quat. Res., 35, pp. 427-437.
Starratt, S.W., 2009, Holocene climate on the Modoc Plateau, northern California, USA: the view from the Medicine Lake: Hydrobiologia, 631, pp. 197-211.

Steponaitis, E., Andrews, A., McGee, D., Quade, J., Hsieh, Y., Broecker, W.S., Shuman, B.N., Burns, S.J., and Cheng, H., 2015, Mid-Holocene drying of the U.S. Great Basin recorded in Nevada speleothems: Quat. Sci. Rev., 127, pp. 174-185.

Swain, D.L., Tsiang, M., Haugen, M., Singh, D., Charland, A., Rajaratnam, B., and Diffenbaugh, N.S., 2014: The Extraordinary California Drought of 2013/2014: Character, Context, and the Role of Climate Change. In: Explaining Extremes of 2013 from a Climate Perspective. *Bull. Amer. Meteor. Soc.*, 95 (9), S3-S7.

Taylor, K.E., Stouffer, R.J., and Meehl, G.A., 2012, An Overview of CMIP5 and the Experiment Design. *Bull. Amer. Meteor. Soc.*, **93**, 485–498. DOI: http://dx.doi.org/10.1175/BAMS-D-11-00094.1

Thompson, R.S., 1984, Late Pleistocene and Holocene Environments in the Great Basin: Ph.D. dissertation, University of Arizona, Tucson.

Thompson, R.S., Whitlock, C., Bartlein, P.J., Harrison, S.P., and Spaulding, W.G., 1993, Climatic Changes in the Western United States since 18,000 yr B.P. In Wright, H.E., Jr., Kutzbackm J.E., Webb, T. III., Ruddiman, W.F., Street-Perrott, F.A., and Bartlein, P.J., editors, *Global climates since the last glacial maximum*, Minneapolis, Minnesota: University of Minnesota Press, 468-513.

U.S. Census Bureau *State and County QuickFacts*, accessed 1 Feb 2016. www.census.gov/quickfacts/table/PST045215/00.

U.S. Department of Agriculture Economic Research Service *State Fact Sheets*, accessed 1 Feb 2016. http://www.ers.usda.gov/data-products/state-fact-sheets/state-data.aspx.

Van Devender, T.R., 1987, Holocene vegetation and climate in the Puerto Blanco Mountains, southwestern Arizona: Quat. Res., 27, pp. 51-72.

Van Devender, T.R., Betancourt, J.B., and Wimberly, M., 1984, Biogeographic implications of a packrat midden sequence from the Sacramento Mountains, south-central New Mexico: Quat. Res., 22, 344-360.

Waddington, J.C.B., and Wright, H.E., Jr., 1974, Late Quaternary vegetational changes on the east side of Yellowstone National Park: Quat. Res., 4, pp. 175-184.

Wagner, J.D.M., 2006, Speleothem Record of Southern Arizona Paleoclimate: U. Arizona. Ph.D. dissertation.

Wahl, E.R., 2002, Paleoecology and testing of paleoclimate hypotheses in southern California during the Holocene: Ph.D. dissertation, U. Minnesota.

Walsh, M.K., Pearl, C.A., Whitlock, C., Bartlein, P.J., and Worona M.A., 2010, An 11,000-year-long record of fire and vegetation history at Beaver Lake, Oregon, central Willamette Valley: Quat. Sci. Rev., 29, pp. 1093-1106.

Waters, M.R., 1989, Late Quaternary lacustrine history and paleoclimatic significance of pluvial Lake Cochise, south-eastern Arizona: Qat. Res., 32, pp. 1-11.

Weng, C., and Jackson, S.T., 1999, Late Glacial and Holocene vegetation history and paleoclimate of the Kaibab Plateau, Arizona: Palaeogeogr., Palaeoclimatol., Palaeoecol., 153, pp. 179-201.

West, G. J. 2004. A late Pleistocene – Holocene pollen record of vegetation change from Little Willow Lake, Lassen Volcanic National Park, California. 65–80. *In* Starratt, S. W. and N. L. Blomquist, editors. Proceedings of the 20th Annual Pacific Climate Workshop. Interagency Ecological Program for the San Francisco Estuary, Technical Report 72.

Wise, E.K., 2010, Spatiotemporal variability of the precipitation dipole transition zone in the western United States: *Geophys. Res. Lett.*, 37, L07706, DOI: 10.1029/2009/GL042193.

Whitlock C., Sarna-Wojcicki, A.M., Bartlein, P.J., and Nickmann, R.J., 2000, Environmental history and tephrostratigraphy at Carp Lake, southwestern Columbia Basin, Washington, USA: Palaeogeogr., Palaeoclimatol., Palaeoecol., 155, pp. 7-29.

Wigand, P.E., and Mehringer, P.J., Jr., 1985, The Archaeology of Hidden Cave, Nevada: Anthropological Papers of the American Museum of Natural History, 61, pp. 108-124.

Worona, M.A., and Whitlock, C., 1995, Late Quaternary vegetation and climate history near Little Lake, central Coast Range, Oregon: GSA Bulletin, 107, pp. 867-876.